Project WP 1627

Development and Application of Novel Sampling Methodologies for Study of Volatile Particulate Matter in Military Aircraft Emissions

Meng-Dawn Cheng

September 2012

Prepared for
U.S. Department of Energy
Environmental Sciences Division
Oak Ridge National Laboratory

Prepared by
OAK RIDGE NATIONAL LABORATORY
Oak Ridge, Tennessee 37831
Managed by
UT-BATTELLE
For the
U.S. DEPARTMENT OF ENERGY
under contract DEAC-05-00OR22725

REPORT DOCUMENTATION PAGE

Form Approved
OMB No. 0704-0188

PLEASE DO NOT RETURN YOUR FORM TO THE ABOVE ADDRESS.

1. REPORT DATE *(DD-MM-YYYY)*	2. REPORT TYPE	3. DATES COVERED *(From - To)*
11-27-2012	FINAL	March 2008 - September 2012

4. TITLE AND SUBTITLE

Development and Application of Novel Sampling Methodologies for Study of Volatile Particulate Matter in Military Aircraft Emissions

5a. CONTRACT NUMBER

5b. GRANT NUMBER

5c. PROGRAM ELEMENT NUMBER

6. AUTHOR(S)

Meng-Dawn Cheng

5d. PROJECT NUMBER

WP-1627

5e. TASK NUMBER

5f. WORK UNIT NUMBER

42

7. PERFORMING ORGANIZATION NAME(S) AND ADDRESS(ES)

Oak Ridge National Laboratory
1 Bethel Valley Road, MS 6038
Oak Ridge, TN 37831-6038

8. PERFORMING ORGANIZATION REPORT NUMBER

ORNL/TM-2012/377

9. SPONSORING/MONITORING AGENCY NAME(S) AND ADDRESS(ES)

Strategic Environmental Research and Development Program
901 N. Stuart Road
Arlington, VA 22203

10. SPONSOR/MONITOR'S ACRONYM(S)

SERDP

11. SPONSOR/MONITOR'S REPORT NUMBER(S)

12. DISTRIBUTION/AVAILABILITY STATEMENT

Approved for public release; distribution is unlimited.

13. SUPPLEMENTARY NOTES

14. ABSTRACT

Understanding the contribution of aircraft emissions to atmospheric particles starts with accurate measurement of volatile particles in the engine exhaust. We focused on the development of an advanced sampling and measurement system consisting of a dilution chamber (DC) and vapor-particle separator (VPS). Results using monodisperse synthetic particles indicate nonvolatile nanoparticles evaporated through sublimation thus their population size remained unchanged but the number concentration decreased as the temperature increased. Volatile particles shrink and evaporate thereby reducing both the particle population size and number concentration. The results unequivocally apply to both particles from conventional diesel compression and turboshaft engine emissions. The VPS could also be used to generate thermogram that can be used to derive evaporation kinetics and energy barrier; both are fundamental quantities of the thermal behavior of an aerosol population.

15. SUBJECT TERMS

Military aircraft emission, particulate matter, volatile particles, JP-8, Fischer-Tropsch, aerosol volatility

16. SECURITY CLASSIFICATION OF:			17. LIMITATION OF ABSTRACT	18. NUMBER OF PAGES	19a. NAME OF RESPONSIBLE PERSON
a. REPORT	b. ABSTRACT	c. THIS PAGE			Meng-Dawn Cheng
U	U	U	UU	75	19b. TELEPHONE NUMBER *(Include area code)* 865-241-5918

TABLE OF CONTENTS

TABLE OF CONTENTS **3**
LIST OF TABLES **4**
LIST OF FIGURES **5**
LIST OF ACRONYMS **7**
LIST OF KEYWORDS **10**
ACKNOWLEDGEMENTS **11**
DISCLAIMERS **11**
ABSTRACT **1**
OBJECTIVES **2**
(I) BACKGROUND **3**
(*I.1*) Description of Volatile Particles and Theory of Vapor-Particle Partition 4
(*I.1.1*) Partitioning 5
(*I.1.2*) Evaporation 6
(*I.2*) Current State of Sampling and Measurement Technology for Volatile Particles 8
(*I.3*) Instruments and Methodology 9
(I.3.1) Differential Mobility Analyzer (DMA) 9
(I.3.2) Condensation Particle Counter (CPC 11
(I.3.3) Scanning Mobility Particle Sizer (SMPS) 11
(I.3.4) Aerosol generation by Nebulizer 11
(II) CONSTRUCT OF THE EXPERIMENTAL SYSTEM **12**
(II.1) Design Rationale 13
(II.2) Dilution Chamber (DC) 14
(II.3) Vapor-Particle Separator (VPS) 17
(III) RESULTS AND DISCUSSION **23**
(III.1) Dilution Chamber 23
(III.1.1) C-17 (F117-PW-100 Engine) Tests 23
(III.1.2) DC-8 (CFM56-2 Engine) Tests 26
(III.2) Vapor-Particle Separator 27
(III.2.1) Tests of VPS Using Laboratory-Generated Particles 27
(III.2.1.1) Particle Penetration Efficiency 28
(III.2.2) Effects of Heating Temperature on Particles 30
(III.2.2.1) Effect of Temperature on Nonvolatile Particle Population 32
(III.2.2.2) Thermal Effect on Volatile Particle Population 35
(III.2.2.3) Rate of Thermal Removal of Nanoparticles 38
(III.2.2.4) VPS Applications in Engine Particles 39
(III.2.2.5) Thermal evolution of diesel engine particles under CDC operating mode 42
(III.3) Tests of DC-VPS Integrated System Using T63 Engine-Generated Particles 45
(IV) CONCLUSIONS **47**
(V) POTENTIAL FUTURE APPLICATIONS **48**
(VI) REFERENCES **49**
APPENDIX A - LIST OF PUBLICATIONS **54**
(A.1) Journal Publication and Technical Reports 54
(A.2) Patent Application and Intellectual Properties 54
(A.3) Professional Presentations 54

LIST OF TABLES

Table 1. Statistical Summary for Particle Number Concentration in CDC Data..... 44
Table 2. Statistical Summary of Particle Diameter in CDC Data..... 45

LIST OF FIGURES

Figure 1. [Adopted from Salo, 2011] Example of a collection of SVOC (precursors: α-pinene ozonolysis products) with total mass concentration shown with a full bars and the condensed phase shown with filled (green) bars based on their logarithmic saturation concentration (log C*)..... 6
Figure 2. Computer drawing of a long-DMA. This is the DMA implemented in the SMPS system shown in Figure 4. 10
Figure 3. A photo of the nano-DMA that can be used in replace of the long-DMA in Figure 2 10
Figure 4. Photo of TSI SMPS system 10
Figure 5. Photo of TSI 3076 atomizer for aerosol generation 12
Figure 6. Illustration of reconfigurable WP1627 sampling and measurement prototype for volatile engine particles 13
Figure 7. Computer Drawing of Dilution Chamber (a) and Implementation of DC for Sampling from T63 Engine..... 15
Figure 8. Axis-symmetric cross-section modeling for dilution chamber design (Dilution Ratio: 100:1) 16
Figure 9. Measured CO2 Concentration in DC at 3 radial and axial locations 17
Figure 10. Computer drawing of the heating section of the VPS 18
Figure 11. Axial temperature profiles of the VPS heating operation 19
Figure 12. Computer drawing of the membrane section of the VPS showing the enclosure of the membrane tube..... 20
Figure 13. SEM micrograph of the membrane surface (a), dimension of a tube (b), and illustration of the double layer structure (adapted from Phelps et al., 2008)..... 20
Figure 14. Photo of the interior of the VPS. 22
Figure 15. Photo of the exterior of the VPS..... 22
Figure 16. Photo of the sampling rake setup for C-17 emissions test. The probes are located at the top of the rake. 24
Figure 17. Average PM measurement in F117 engine at several power settings for probe-tip and N2-diluted DC: (a) upper panel the particle number EI, and (b) lower panel the particle size distribution 25
Figure 18. Impacts of PM dilution techniques on particle number EI and size distribution for CFM56-2 engine during the NASA-sponsored AAFEX II tests JP-8 27
Figure 19. Experimental setup for VPS evaluation using synthetic particles in laboratory conditions..... 28
Figure 20. Size distribution for DOP particles through the by-pass and VPS. Two curves virtually overlapping each other. 29
Figure 21. Setup of Tandem DMA in generating monodisperse particles for challenging VPS 31
Figure 22. Size distribution of monodisperse NaCl particles in response to temperature variation in VPS..... 33
Figure 23. Size distribution of monodisperse DOP particles as a function of temperature 36
Figure 24. Evaporation kinetics of various nanoparticles..... 39

Figure 25. TDMA setup for diesel engine experiment at NTRC 40
Figure 26. Photo of the diesel engine apparatus at NTRC 41
Figure 27. Photo of the TDMA-VPS setup at NTRC 41
Figure 28. Size distribution of monodisperse CDC engine particles in response to temperature variation in VPS (a=95nm, b=52nm, c=18nm) 44
Figure 29. Size distributions of particles taken during an idle T63 engine operation 46
Figure 30. Size distributions of cruise T63 engine emissions 46

LIST OF ACRONYMS

AAFEX	Alternative Aviation Fuel Experiment
CFD	Computational Fluid Dynamics
CDC	Compression Diesel Compression
CPC	Condensation Particle Counter
CVS	Constant Volume Sampling
DCLA	Diffusion-Limited Cluster Aggregate
DEED	Dekati Engine Exhaust Diluter
DMA	Differential Mobility Analyzer
DOD	Department of Defense
DOE	Department of Energy
DOP	Dioctyl Phthalate
DC	Dilution Chamber
EEP	Engine Exhaust Plane
EI	Emission Index, same as EF in this report
EM	Electron Microscopy; also see TEM and SEM
EPA	Environmental Protection Agency
ESS	Emission Sampling System from Grimm Aerosol Technik
ESTCP	Environmental Security Technology Certification Program
FSC	Fuel Sulfur Content, usually in units of parts-per-million by weight or ppmw
GM	Geometric Mean Diameter in nm
GSD	Geometric Standard Deviation in nm
HC	Hydrocarbons
HEFA	Hydroprocessed Esters and Fatty Acid
JP-8	Jet Propellant, Jet fuel

LPM	Litter per Minute
MBTCA	3-methyl-1,2,3-butanetricarboxylic acid
MFC	Mass Flow Controller
MFIX	Multiphase Flow with Interface Exchange (a DOE software)
NIOSH	National Institute for Occupational Safety and Health
NTRC	National Transportation Research Center
NVPM	Nonvolatile Particulate Matter
OC/EC	Organic Carbon/Elemental Carbon
ORISE	Oak Ridge Institute of Science and Education
ORNL	Oak Ridge National Laboratory
PAH	Polyaromatic Hydrocarbons
PM	Particulate Matter
PMP	Particle Measurement Protocol
PNC	Particle Concentration Counter
PSD	Particle Size Distribution
RH	Relative Humidity
SAE	Society of Aeronautics Engineering
SERDP	Strategic Environmental Research and Development Program
SMPS	Scanning Mobility Particle Sizer
SOA	Secondary Organic Aerosol
SVOC	Semi-Volatile Organic Compounds
TDMA	Tandem Differential Mobility Analyzer
THCs	Total Hydrocarbons
TERTEL	Turbine Engine Research Transportable Emissions Lab
TSP	Total Suspended Particulate
UCPC	Ultrafine Condensation Particle Counter

UDRI	University of Dayton Research Institute
US EPA	United States Environmental Protection Agency
VBS	Volatility Basis Set
VPM	Volatile Particulate Matter
VPR	Volatile Particle Remover
VPS	Vapor-Particle Separator
VTDMA	Volatility Tandem Differential Mobility Analyzer
WFO	Work for Others
WP AFRL	Wright-Patterson Air Force Research Laboratory

LIST OF KEYWORDS

Aircraft

Diesel

Dilution

Emission

Fischer-Tropsch

FTIR

JP-8

Mobility

Particles

Particulate Matter

Sampling

Turboshaft

Ultrafine

Volatility

Volatile Particles

ACKNOWLEDGEMENTS

This project was financially supported in part by the Department of Defense Strategic Environmental Research and Development Program (SERDP) under the project number WP1627, the Department of Energy SULI graduate students program, the National Science Foundation Graduate Fellowship program, and the Department of Energy Heavy Vehicle Research Program.

The SERDP project WP1627 team consists of the following members (listed in alphabetical order of the last name): Steve Allman (ORNL), Meng-Dawn Cheng (ORNL), Edwin Corporan (AFRL), Matthew DeWitt (UDRI), Christopher Klingshirn (UDRI), and Richard Steinbach (UDRI).

Dr. Meng-Dawn Cheng is the Principal Investigator (PI) of this project, and Mr. Edwin Corporan is the Co-PI of this project.

Computational simulations, data analysis, technical discussions, laboratory experiments and field test campaigns performed throughout this research project could not be successful without the support of the following dedicated persons:

Alejandro M. Briones (UDRI), Teresa Barone (ORNL), Brian Bischoff (ORNL), Scott Curran (ORNL), Brian Damit (Univ. Florida - Gainesville), Tommy Phelps (ORNL), Bradley Landgraf (University of Pennsylvania), Shannon Mahurin (ORNL), Tommy Phelps (ORNL), and John Storey (ORNL)

Interactions, joint field campaigns, technical discussions, and team meetings during the annual SERDP symposium among the three volatile engine particle teams (WP1625, WP1626, and WP1627) have been beneficial for this project. The PI and Co-PI acknowledges Dr. Richard Miake-Lye of Aerodyne for coordinating the annual SERDP VPM meetings.

Oak Ridge National Laboratory, in coordination with the Air Force Research Laboratory at Wright-Patterson Air Force Base, assumed the lead organization responsibility for planning, execution of the project, and preparation of this final report.

Oak Ridge National Laboratory is managed by UT-Battelle, LLC, for the U.S. Department of Energy under contract DE-AC05-00OR22725.

DISCLAIMERS

The mention of commercial instruments, model numbers, trade names, chemicals and chemical manufacturers do not represent the endorsement of the author and other SERDP WP 1627 team members nor the organizations the author and team members are associated with.

THIS PAGE IS INTENTIONALLY LEFT BLANK.

ABSTRACT

Understanding the contribution of aircraft emissions to atmospheric particles starts with accurate measurement of volatile particles in the engine exhaust. We focused on the development of an advanced sampling and measurement system consisting of a dilution chamber (DC) and vapor-particle separator (VPS). Results using monodisperse synthetic particles indicate nonvolatile nanoparticles evaporated through sublimation thus their population size remained unchanged but the number concentration decreased as the temperature increased. Volatile particles shrink and evaporate thereby reducing both the particle population size and number concentration. The results unequivocally apply to both particles from conventional diesel compression and turboshaft engine emissions. The VPS could also be used to generate thermogram that can be used to derive evaporation kinetics and energy barrier; both are fundamental quantities of the thermal behavior of an aerosol population.

OBJECTIVES

The objectives of this project were: (1) to improve understandings of volatile particles in military aircraft engines and other type of fossil fuel combustions, (2) to develop a new sampling system that resolves current sampling difficulty of using a tip-dilution probe, and (3) to develop a novel instrument for precision measurement of engine particulate volatility.

(I) BACKGROUND

Aircraft emissions contribute to the increase of NO_x, volatile organic compounds, and particulate matter (PM) in the atmosphere. Since aircraft directly inject pollutants into the atmosphere, its engine emissions play a significant role in the alteration of atmospheric chemistry, the life cycles of cloud nuclei and contrails that play a critical role in climate forcing and radiation balance [Intergovernmental Panel on Climate Change (IPCC), 2007; http://www.ipcc.ch/]. On the ground, aircraft emissions add to the pollution load in an airshed, which could endanger the continuous operation of a military base if the base is located in a non-compliance area such as a large metropolitan area that is in violation of the National Ambient Air Quality Standards (NAAQS; http://www.epa.gov/air/criteria.html). NAAQS were specifically designed to protect human health and environmental well being against excessive levels of ozone, sulfur and nitrogen oxide, lead, and particulate matter of 10 and 2.5 μm in the ambient air. Aircraft emissions are known to have adverse impacts on human health caused by the soot particles and hazardous compounds (e.g., formaldehyde, polyaromatic hydrocarbons) emitted as the by-product of engine fuels and lubricants.

Considering PM emissions as an example, the aircraft fleet-averaged emission index for soot has been estimated to be approximately 40 mg/kg of fuel burned [International Civil Aviation Organization (ICAO) Data Base]. This renders approximately 600,000 kg of particulate matter, which are emitted each year by US military aircraft alone. However, the portion of the emissions contributed to each aircraft platform is unknown. The level of emissions from military engines corresponds roughly to $5x10^{24}$ particles per year with an average size of 50-nm diameter and an average density of $2g/cm^3$ (Howard, 1996). Military aircraft emissions are dominated by a fleet of high payload aircraft, such as the C-130, B1 B-52, and a variety of heavy-lift turboshaft vehicles used across the services by the US Armed Force. These aircraft consume the majority (60-70%) of fuel used by the US Air Force (USAF) alone due to their large payloads, frequent flight missions and older engine technology; i.e., lower-efficiency engines. For example, smoke numbers for these aircraft are in the 30s or 40s, while fighter jets are typically in the single digits range that is near the detection limit of smoke number. The USAF intends to continue operation of these aircraft for the foreseeable future (e.g., the B-52 aircraft is expected to remain in service until about 2050).

A document has been published recently (AIR 5892, 2012) by the SAE International E31 Committee as a standard for sampling and measurement of aircraft nonvolatile particles. This enables standardized aircraft emission tests for nonvolatile particles. Nonvolatile particles are commonly considered as soot, which is black carbon and exist mostly as particulate matter in the ambient conditions. Soot has a robust structure and high melting point. Depending on the combustion conditions, soot can have a highly complex morphological structure called the fractal structure, which is commonly characterized by the fractal dimension. For example, soot particles produced by combustion of hydrocarbon fuel (e.g., ethylene) generally has a fractal dimension of 1.8. These structures are commonly called the diffusion-limited cluster aggregate (DCLA) and have been known for a couple of decades (e.g., Sorensen et al., 1992). DCLA exists also in engine particles (e.g., Maricq and Xu, 2004). According to Particle Measurement Programme (PMP) recommendations (Andersson and Clarke, 2004), the nonvolatile particle number measurement system must sample from a constant volume sampler (CVS) 10 to 20 tunnel diameters downstream of the gas inlet. The number measurement system will comprise a sample pre-conditioning unit (or volatile particle remover) upstream of a particle number concentration counter (PNC).

A particle size pre-classifier (e.g., cyclone, Impactor, etc.) prior to the inlet of the sample pre-conditioning unit is recommended. According to PMP recommendations (Andersson and Clarke, 2004), the sample pre-conditioning unit

- shall be capable of diluting the sample in one or more stages to achieve a particle number concentration below the upper threshold of the single-particle count mode of the PNC (usually 10^4 cm^{-3}) and a gas temperature below 35°C at the inlet to the PNC;
- shall include an initial heated dilution stage with dilution of >10:1 which outputs a diluted sample at a temperature of 150–400°C;
- shall achieve >99% reduction of an aerosol comprising 30 nm tetracontane ($CH_3(CH_2)_{38}CH_3$) with inlet concentration of $>10^4$ cm^{-3} by means of heating and reduction of partial pressures of the tetracontane;
- shall include elements which operate under conditions that achieve greater than 60, 70 and 80% solid particle penetration respectively at 30, 50 and 100 nm particle diameters for the sample pre-conditioning unit as a whole.

With the precisely specified requirements for measurement of nonvolatile engine particles, there was no such specification for measurement of volatile engine particles. Sulfuric and organic constituents in the aircraft fuels are two major sources of volatile particles. The by-products from combustion of these two classes of fuel materials could lead to species that are in the gas or vapor phase at the engine exhaust plane (EEP), but subsequently found to be on the particulate phase when these gas-phase species immerse into the ambient environment downstream after the EEP. In fact, it has been known for more than a decade or two ago that sulfuric acids resulted from combustion of sulfur in fuel and emission of sulfur dioxide and sulfite promote the formation of contrail at higher altitude (e.g., Schumann et al., 2002; Busen and Schumann, 1995). Many reactive organic compounds (discussed in textbook like Seinfeld and Pandis, 2006) are known to cause ozone formation through photochemical reactions and production of fine particles like smog, which was discovered in the 1970s. Smog is also called secondary aerosol and is formed in the atmosphere by chemical reactions of the man-made and natural species called precursor species. Secondary aerosol is a major component of atmospheric aerosol in many airshed throughout the US and around the world (e.g., Robinson et al., 2007). In fact, more than 85% of the PM mass in the Southeastern US is secondary aerosol (Zheng et al., 2002). However, how much of the secondary aerosol is caused by the military aircraft emissions remained to be learned, because measurement of volatile engine particles has been more challenging than that of nonvolatile ones. There is no standard or well accepted method for sampling and measurement of volatile particles emitted by military aircraft engines.

(*I.1*) Description of Volatile Particles and Theory of Vapor-Particle Partition

Particulate emissions from an aircraft engine are classified as nonvolatile and volatile particles based on thermal differentiation terminology. It is an operationally defined term. Sampling at the engine exhaust plane (about 1 m from the nozzle), those that can be measured by current aerosol detection technology are called the “primary” or “nonvolatile” particles. The volatile particles that are unique signature of engine emission are normally found at a condition when condensation, nucleation, and gas-to-particle conversion processes occur. These are typically downstream from the engine exhaust plane. Secondary organic aerosols (SOA), generated from the above-mentioned processes, are an important component of atmospheric aerosols. For example, approximately 70-80% of the PM mass found in the Southeast region of the US is SOA (Zheng et al., 2002). Robinson et al. (2007 & 2011) and many others reported that aircraft emissions could be a major factor contributing to the formation of SOA in an airshed. SOA exists only in ambient condition, and it has not been detected at the engine exhaust plane simply because it does not exist as particulate matter under the condition at the exhaust plane. SOA is thus qualified as a volatile particle.

There are other volatile particles exist in the aircraft engine exhaust. Sulfur-based particles, for example, have been found not only in the ambient particles but also in the exhaust at EEP (Cheng et al.,

2010). Sulfur is an important ingredient of aircraft fuel due to its ability to lubricate and seal. Thermodynamics of sulfur compounds dedicate that they exist only in the vapor phase, mostly as SO_2 in the engine combustion condition. SO_2 is converted to sulfite (SO_3), which is highly hygroscopic. Conversion to sulfate is almost instant once the sulfur-based species mixes with the ambient air containing water vapor. Homogeneous and heterogeneous nucleation form new sulfur-based particles, while heterogeneous condensation lead to addition of mass to existing aerosol particles. All these aerosol dynamics change the size distribution of aerosol particles. Gas-to-particle conversion and gas/particulate partition follows the law of thermodynamics; thus, species such as sulfate is commonly found in atmospheric aerosol downstream of an aircraft emission. Projects like SULFUR (Schumann et al., 2002) have demonstrated the existence of sulfate particles in the cruising altitude of an aircraft. Cheng et al. (2009) have also reported significant quantity of sulfate, measured by ion chromatograph, on particulate samples collected only a few meters downstream from a T700 turboshaft engine used by US Army in the helicopter fleet. Aerosol volatility, which determines the existence of volatile particles, is controlled by the thermodynamic partition.

(*I.1.1*) Partitioning

The distribution of a semi-volatile organic compound (SVOC) between the gaseous and condensed phase in the atmosphere is often described with the partitioning coefficient Kp (Pankow, 1994).

(1) $$K_{p,i} = \frac{F_{i,om}}{A_i TSP} = \frac{RTf_{om}}{MW_{om}\zeta_i p_i^0}$$

Where $F_{i,om}$ and A_i are the condensed and gaseous concentrations of compound i and TSP is the concentration of the total suspended particulate matter. R is the common gas constant, T the temperature, f_{om} is the weight fraction of the TSP that is the absorbing organic material, MW_{om} the mean molecular weight of the absorbing organic material, ζ_i is the activity coefficient and p^0_i is the saturation vapor pressure. Equation (1) shows that an SVOC will distribute between the condensed and gaseous phase not only depending on temperature and molecular properties, but also on the total aerosol concentration. Eq. (1) has been applied conventionally for atmospheric aerosol. Its practical form in the functional of Eq. (1) is believed to be applicable to the phase partition of a SVOC of turbine engine origin. This implies that the dilution of an engine exhaust thereby reducing TSP in the exhaust will change the particle chemical composition by forcing compound i to go into the gas phase from the particulate phase. To infer this further, a tip-dilution probe would force a SVOC to leave the particulate phase thereby leading to a stable particle population by reducing (1) the opportunity of forming particles through nucleated condensation and (2) the chance of coagulation through reduction of the number concentration of particles.

Another technical approach to describe the volatility distribution of the compounds in an aerosol is the Volatility Basis Set (VBS) as described by Donahue et al. (2006). The basis for this method is to lump the vast number of secondary organic aerosol (SOA) constituents into "volatility bins". These bins are based on saturation vapor pressures of the different compounds, often expressed as Ci* ($\mu g\ m^{-3}$) and separated by factors of 10. The bins often range from 0.01 to 100,000$\mu g\ m^{-3}$ covering the least volatile compounds in the atmosphere (entirely in the condensed phase under atmospheric conditions) to the most volatile (entirely present in the gaseous phase). The unit is dependent on the molecular weight, but it is assumed that the constituents have a mean molecular weight of ~ 200 $g\ mol^{-1}$ (Donahue et al., 2006). Adopted from Salo (2011), as an example, Figure 1 shows the volatility distribution of the products from a α-pinene ozonolysis experiment following the VBS approach. The white bars show gas phase compounds and the green bars the products in the condensed phase in the presence of 66.3$\mu g\ m^{-3}$ organic aerosol.

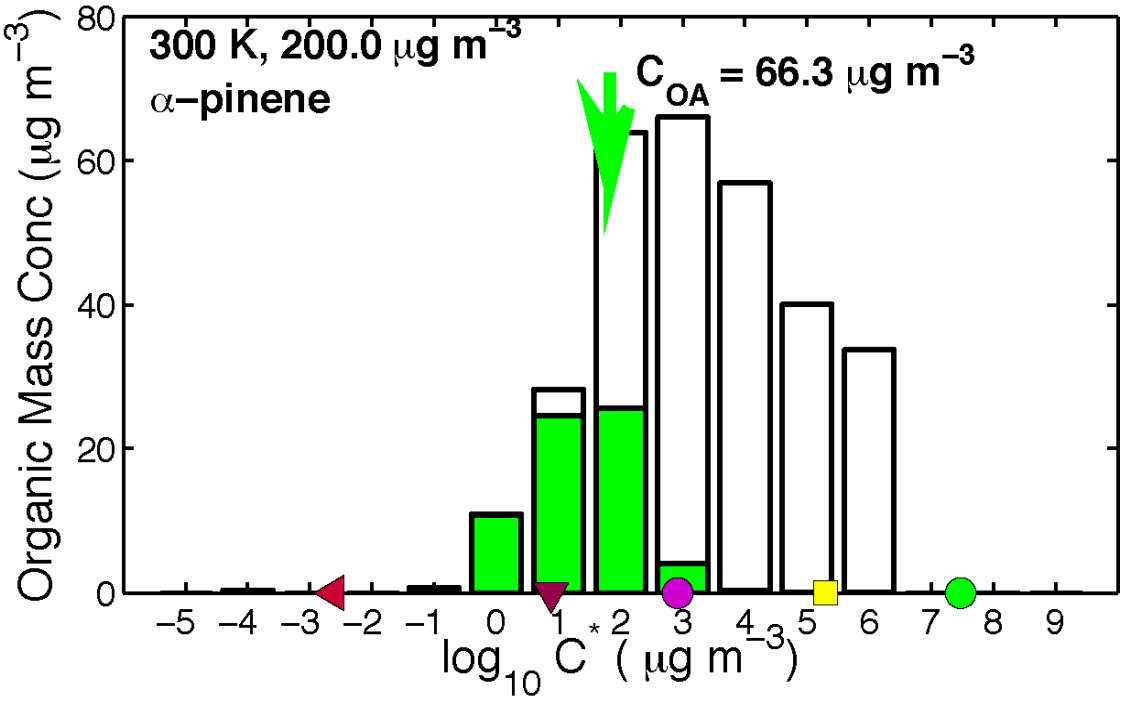

Figure 1. [Adopted from Salo, 2011] Example of a collection of SVOC (precursors: α-pinene ozonolysis products) with total mass concentration shown with a full bars and the condensed phase shown with filled (green) bars based on their logarithmic saturation concentration (log C*).

Green circle is the logarithmic vapor pressure for α-pinene and oxidation products, yellow square is pinonaldehyde, magenta circle is for pinonic acid, maroon downward triangle is for pinic acid, and red leftward triangle is for MBTCA.

(*I.1.2*) Evaporation

The phase transition from a liquid aerosol particle to the gas phase is defined as vaporization and from a solid particle as sublimation. The energy needed to transfer one mole of a compound between the condensed phase and the gaseous phase is called the enthalpy of vaporization/sublimation. The volatility of a SOA particle is dependent on its phase, composition and the interactions between its constituents including the carrier gas. In this final report the word, evaporation or vaporization, will be used synonymously with sublimation or vaporization to describe the gas transition from amorphous or unknown phases.

The evaporation from an aerosol particle consisting of a single compound can be described based on the assumptions that (1) the particle is spherical with isotropic surface free energy and (2) the vapor pressures from the evaporated species and any latent heat are negligible. The change of particle size through evaporation is described as:

$$\frac{dD_p}{dt} = -\frac{4D_{i,air}M_i}{\rho_i D_p RT} p_i^0 \exp\left(\frac{4\gamma_i M_i}{D_p \rho_i RT}\right) f(Kn_i, \alpha) \quad (2)$$

Where D_p is the particle diameter, $D_{i,air}$ is the diffusivity of compound i in air. M_i is the molar mass of i and ρ_i is the density. R the gas constant, T the temperature, t the evaporation time and γ_i is the surface free

energy. $f(\mathrm{Kn_i}, \alpha)$ is the semi empirical Fuchs and Sutugin correction term for particle diameters in the non continuous; e.g., transition regime (Fuchs and Sutugin, 1971).

$$f(Kn_i,\alpha) = \frac{1+Kn_i}{1+0.3773\times Kn_i + 1.33\times Kn_i \times \frac{(1+Kn_i)}{\alpha}} \quad (3)$$

Where α is the mass accommodation or evaporation factor, in the case of evaporation, this factor describes the inertia (in the form of coefficient) in the evaporation process. Recent publications discuss the magnitude of this quantity in the atmospheric particle evaporation processes (Riipinen et al., 2010; Vaden et al., 2011). $\mathrm{Kn_i}$ is the Knudsen number, a dimensionless number defined in Equation 3. It is the ratio between the mean free path (λ) and the particle diameter (Dp). A $\mathrm{Kn_i} \rightarrow 0$ indicates continuum regime, $\mathrm{Kn_i} \rightarrow \infty$ free molecule (kinetic) regime, while a $\mathrm{Kn_i} \sim 1$ indicates that the mass flux occurs in the transition regime. The mean free path λ_{air} (@ 298K) is 66 nm meaning that 10 nm < Dp < 200 nm, like most of nonvolatile engine particles, would belong to the transition regime (Seinfeld and Pandis, 2006).

The diffusivity of species i in air, $\mathrm{D_{i,air}}$, is given by

$$D_{i,air} = 5.9542\times10^{24} \frac{\sqrt{T^3\left(\frac{1}{M_i}+\frac{1}{M_{air}}\right)}}{p\sigma_{i,air}^2\Omega_{i,air}}$$

Where $\mathrm{M_i}$ is the molar mass of the $\mathrm{i^{th}}$ species, p is the total pressure and σ_i is the inter-particle distance where the potential is zero derived from the critical volume ($\mathrm{V_{c,i}}$) of i as $\sigma_i = 0.841\ (\mathrm{V_{c,i}})^{1/3}$. The collision integral for i in air ($\Omega_{i,air}$) was calculated as described by Bird and Stewart (Bird et al. 1960) in mass transfer theory using the Lennard-Jones parameter $\varepsilon_{i,air}$ which is the depth of the potential energy well for the molecule i in air. ε is calculated from the melting temperature (Tm) as $\varepsilon_i = 1.92$ Tm (Bird et al. 1960). $\varepsilon_{i,air}$ and $\sigma_{i,air}$ was calculated as described in Equation 4, using $\sigma_{air} = 3.617$ Å and $\varepsilon_{air} = 97$ K.

$$\sigma_{i,air} = \frac{\sigma_{i,i}+\sigma_{air}}{2}$$
$$\varepsilon_{i,air} = \sqrt{\varepsilon_{ii}\times\varepsilon_{air}} \quad (4)$$

The integrated form of Equation 2 was used to calculate the saturation vapor pressure (p^0) at each temperature.

$$p^0 = -\frac{\rho_i RT}{4D_{i,air}\Delta t M_i}\int_{Dp,i}^{Dp,f}\frac{D_p}{f(Kn_i,\alpha)}\exp\left(\frac{-4\gamma_i M_i}{D_p\rho_i RT}\right)dD_p \quad (5)$$

In Eq. (5), $\mathrm{D_{p,i}}$ is the initial and $\mathrm{D_{p,f}}$ is the final particle diameter after evaporation. Δt is the evaporation time corrected for the temperature effect on the volume flow rate. Using Equation 5 and the assumptions above p^0 of a compound was calculated for an extended temperature range using the evaporation rate. Assuming the enthalpy of evaporation was constant over the whole temperature range the Clausius-Clapeyron relationship [Eq. (6)] was used to calculate the enthalpy of evaporation (ΔH_{evap}) and the p^0 at 298K was inferred using extrapolation.

(6) $$\frac{d \ln p^{\circ}}{d\left(\frac{1}{T}\right)} = -\frac{\Delta H^{0}}{R}$$

Since the method described here utilizes the dynamic evaporation that takes place under non-equilibrated conditions, the determination of the evaporation time is critical. The volumetric flow is corrected for the expansion of the air during heating.

(*I.2*) Current State of Sampling and Measurement Technology for Volatile Particles

To remove volatile materials in engine-emitted aerosol so one could measure the nonvolatile particles more accurately, techniques like thermodenuder (Burtscher et al., 2001; Burtscher, 2005; Maricq, 2007), catalytic stripping (Swanson and Kittelson, 2010), and volatility tandem differential mobility analyzer (VTDMA) (Ronkko et al., 2007; Wehner et al., 2002) have been developed. None of these techniques enables one to observe engine particle dynamics, molecular transfer, or evaporation process under varying temperature conditions. For example, the thermodenuder and the catalytic stripper were intended for rapid removal of volatile components from soot particles, while VTDMA was to investigate volatilization and hygroscopicity of single ambient aerosol particles. Although highly detailed, the mobility analyzer design was too slow to be suitable for VPM measurement. In addition, the concentrations of water vapor, unburned hydrocarbons, and particles in engine exhaust are so high that the VTDMA design would not work.

Since 30 years ago, thermodenuder has been a popular device designed to desorb volatile species from studies of ambient particles (Newman, 1978; Cobourn et al., 1978; Slanina et al., 1987; Sturges and Harrison, 1988; Johnson et al., 2004; An et al., 2007; Villani et al., 2007). Thermal stripping devices have also been used on diesel engine soot and aircraft emissions (Fierz et al., 2007; Park et al., 2008; Huffman et al., 2008; Wu et al., 2009). Although volatile components were removed from the particulate matter, the adsorbent used in these designs however retained the volatile components throughout the measurement system (Swanson and Kittelson, 2010). Once the adsorption capacity runs out, the volatiles could and have been found to return to the particles or to form new condensible state (Swanson and Kittelson, 2010). The technique produced serious artifacts (Burtscher, 2005) and how to accurately characterize nonvolatile particles of the engine exhaust has been treated as an instrumentation issue, particularly in diesel engine exhaust research since the 1990s. Two review articles published by Burtscher (2005) and Maricq (2007) described extensively the techniques for physical and chemical characterization of particulate emission from diesel engines. The thermal removal efficiency of a thermodenuder has never been 100% due to the nature of sampling and thermal desorption in the exhaust flow. Distortion of the engine particle size distribution can be severe because loss of particles in the heating system is not uniform across the size range of the particles.

Overall, there are several fundamental issues related to sampling and measurement of engine VPM. In our own study (Cheng, 2010) using commercially available thermodenuders the results indicated the loss of particles ranges from 15% to 85% for 500 and 25 nm particles, respectively. Since the loss is particle size dependent, the loss makes an accurate quantification of source emissions challenging if not impossible. This is a very serious issue when the number of particles is the primary metric in engine emissions control and regulation, for example, in EURO5 (Giechaskiel et al., 2010). Finally, the uses of granulate charcoal adsorbent to remove vapors makes it impossible to extract adsorbed vapors for quantitatively analysis. The high labor required to maintain and replace the charcoal pellets for denuding the engine aerosol stream is not desirable.

Several commercially available volatile particle remover (VPR) were tested in SAMPLE III. These included (1) AVL Particle Counter (APC400), (2) Dekati Engine Exhaust Diluter (DEED), (3) Grimm Emission Sampling System (ESS), (4) bespoke custom made consortium designed VPR and (5) University of Minnesota Catalytic Stripper. The last device is not commercially available. The test results are detailed in the final report for SAMPLE III project (Crayford et al., 2011). Tests were compared among the devices and against the current PMP protocol.

An excerpt summary of their conclusions (Crayford et al., 2011) relevant to this work is presented below:

1. As expected the PMP approved commercially available VPR (i.e., Dekati DEED, AVL APC400) as well as the bespoke consortium designed conform to PMP protocol in terms of laboratory based testing.
2. The Grimm ESS VPR did not meet all of the specifications set out by the PMP, it is thought that the reason for this is the lack of evaporation tube and lower temperatures utilized by the unit.
3. It was found that PMP VPR do not "remove" all of the volatile PM, but shrinks over 99% of the volatile PM to a size below the 23nm cut off selected by PMP. This could lead to large uncertainties particularly if the volatile to nonvolatile PM number ratio is high.
4. Catalytic Stripper technology appeared to completely remove tetracontane and lubrication oil in the form of pure volatile PM and volatile coated carbon particles. It would pass PMP VPR performance specifications, although the Catalytic Stripper does not conform to PMP design specification.
5. Data suggests that PMP type diluters could be "slightly" modified to potentially reduce the attainable lower size cut-off by increasing the primary dilution temperature along with the evaporation tube temperature.
6. During numerous combustor and full scale engine tests in SAMPLE III, volatile particles appear to exist throughout the measureable PM size range and are not only present in the primary nucleation mode peak as current scientific understanding would suggest.

The last finding (#6) suggests that the understanding of engine volatile particles and vapor-particle partition in engine exhaust requires improvement.

(*I.3*) Instruments and Methodology

(I.3.1) Differential Mobility Analyzer (DMA)

The differential mobility analyzer (DMA) is a commonly used instrument to measure aerosol size distributions. It uses the size dependence of the mobility of charged particles in an electrical field to measure the equivalent size of an aerosol particle. A computer drawing of the long DMA is shown in Figure 2. In Figure 3 a photo of the nano-DMA is shown. A polydisperse sample aerosol enters the system through a neutralizer. The neutralized aerosol then enters the cylinder with a charged rod in the center. In the laminar flow region the particles with the opposite charge referencing to the rod will be migrated towards the rod. The drag force the particles experience is proportional to the diameter and shape of the charged particle. Particles of "non-selected" mobility are collected on the charged rod. Particles with an electrical mobility diameter corresponding to the set voltage will pass through the sample slit and form a monodisperse aerosol flow. The technique is highly size selective, and can achieve a resolution at the full-width half-maximum of 3nm in real-world engine operation and less than 1nm in a precision experiment under laboratory-controlled condition. The geometric standard deviation used to quantify the dispersion of the particle size in a particle population is typically less than 1.2 for a DMA selected particle population. Thus, for all practical purpose, a particle population characterized with a geometric standard deviation of 1.2 or less is called monodisperse.

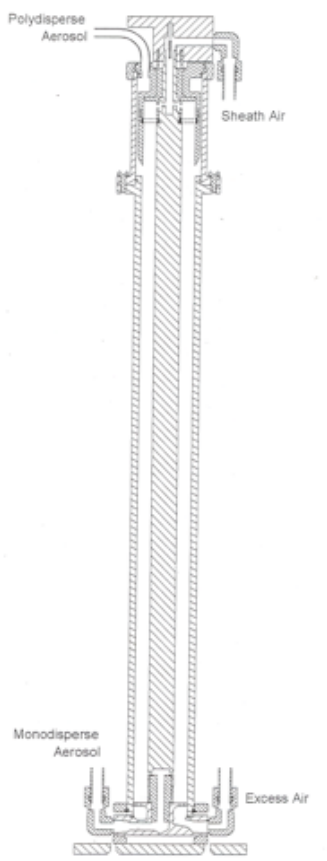

Figure 2. Computer drawing of a long-DMA. This is the DMA implemented in the SMPS system shown in Figure 4.

Figure 3. A photo of the nano-DMA that can be used in replace of the long-DMA in Figure 2

Figure 4. Photo of TSI SMPS system

(I.3.2) Condensation Particle Counter (CPC

Aerosol particles smaller than a couple of hundred nanometers are generally too small to be detected effectively by optical techniques and in order to detect the particles a condensation particle counter (CPC) was used. In the CPC, the aerosol flow is passed through a volume saturated with a working fluid, often water or alcohol (in TSI 3025A 1-butanol was used) and thereafter passed through a cooled volume. When cooled down the working fluid reaches supersaturation and the butanol molecules condense on the particles as the name "condensation particle counter" implies, the particles will grow in size to be large enough to be detectable with laser optical methods. Stepping through the voltage on the center rod of a DMA and the particles exit the DMA are counted with a CPC. Since the voltage is known, the mobility diameter of the particles exiting the DMA is known. Combining the mobility data and the CPC data, a size distribution of particles based on the number concentration can be achieved with a time resolution as short as 60s. Together in an instrument system, the DMA and CPC can make up the working components in a scanning mobility particle sizer (SMPS) system that this project heavily utilized.

(I.3.3) Scanning Mobility Particle Sizer (SMPS)

The SMPS is a system commonly used in aircraft emission measurement and evaluated in many field-sampling campaigns (Cheng et al., 2009; 2010). Figure 4 shows a photo of the SMPS that is equipped with a long DMA and an ultrafine CPC (UCPC, TSI Model 3025A). Aerosol particles enter the SMPS are screened by an impactor at the entrance into the DMA. Particles are neutralized by using an X-Ray ion generation device or a radionuclide device. Both devices impart ions of positive and negative polarity that render the charged population of the particles to become normally distributed. Then a given value of particle mobility is selected by applying a selected voltage to the column inside the DMA, particles of right electrical mobility are extracted, as described in the DMA section earlier, through a slit to be counted by the UCPC. The voltage generally scanned from low (a few hundred volts) to high (a few thousand volts) in a pre-determined cycle over the size range of interest. Data reduction software fuses the scanned voltage data (converting into the mobility diameter) and the particle counts from the UCPC to produce a particle size distribution that is based on the particle number concentration. This instrument has been tested thoroughly in the previous WP 1401 project (Cheng et al., 2008) and found to be reliable for aircraft emissions measurement.

(I.3.4) Aerosol generation by Nebulizer

To generate test aerosols from aqueous solutions of the pure compounds described in Section III.2 the TSI 3076 constant output atomizer was used. This atomizer is a collision-type device that generates aerosols of constant particle size in a number concentration greater than 10^7 cm^{-3}. The atomizer was operated in a non-circulating mode, to minimize the effect of concentration built-up affecting on particle size and number concentration, and fed with dried HEPA-treated particle-free pressurized air from the building supply. The pure compounds were dissolved in deionized water (Nanopure, 18MΩ). The generated aerosol was dried with silica diffusion dryers and diluted to suitable concentrations before entering the size-selection DMA. This method generates an aerosol stream with RH < 5% at the room temperature. Aerosol particles created by this method are generally solid (crystallized) or liquid (such as oil drops from Dioctyl Phthalate) depending on the purity of the sample but also by its physical properties like hygroscopicity, solubility or crystallization rate. Figure 5 shows a picture of the TSI 3076 atomizer.

Figure 5. Photo of TSI 3076 atomizer for aerosol generation

(II) CONSTRUCT OF THE EXPERIMENTAL SYSTEM

This research program focuses on development of a new sampling and measurement system to be deployed at the engine exhaust plane where negligible influence of ambient influence exists. Most of the research works conducted previously for sulfate particles, for example, were performed in downstream of aircraft emissions where mixing of the engine plume and ambient particles is significant. Our intended goal is for this system to be deployable to field use replacing the emission measurement system currently used by WP AFRL for nonvolatile engine particles. The new system has been designed with the idea in mind that it can be used for measurement of nonvolatile particles as well as volatile particles by simply dialing in required conditions.

Figure 6 illustrates the reconfigurable system for sampling and measurement of volatile particles resulted from this research project. The two major components of this system are (1) the dilution chamber (DC) and (2) the vapor-particle separator (VPS). The DC is the sampling front end of the prototype, which was designed with the goals of (a) providing a representative dilution sampling capability, (b) reproducing condensation on-demand, and (c) possibly replacing a tip-dilution probe. The VPS is designed as a high transmission efficiency remover of volatile particles; i.e. an instrument of insignificant particle loss. The goal is to design the VPS such that it has the capability to provide the information regarding particle volatility and thermograph of an aerosol population. In combination, the DC-VPS system would enable the aircraft emission community a tool that can investigate both nonvolatile and volatile particles. Both instruments will be simple to use, robust or rugged in field operation, and user-friendly.

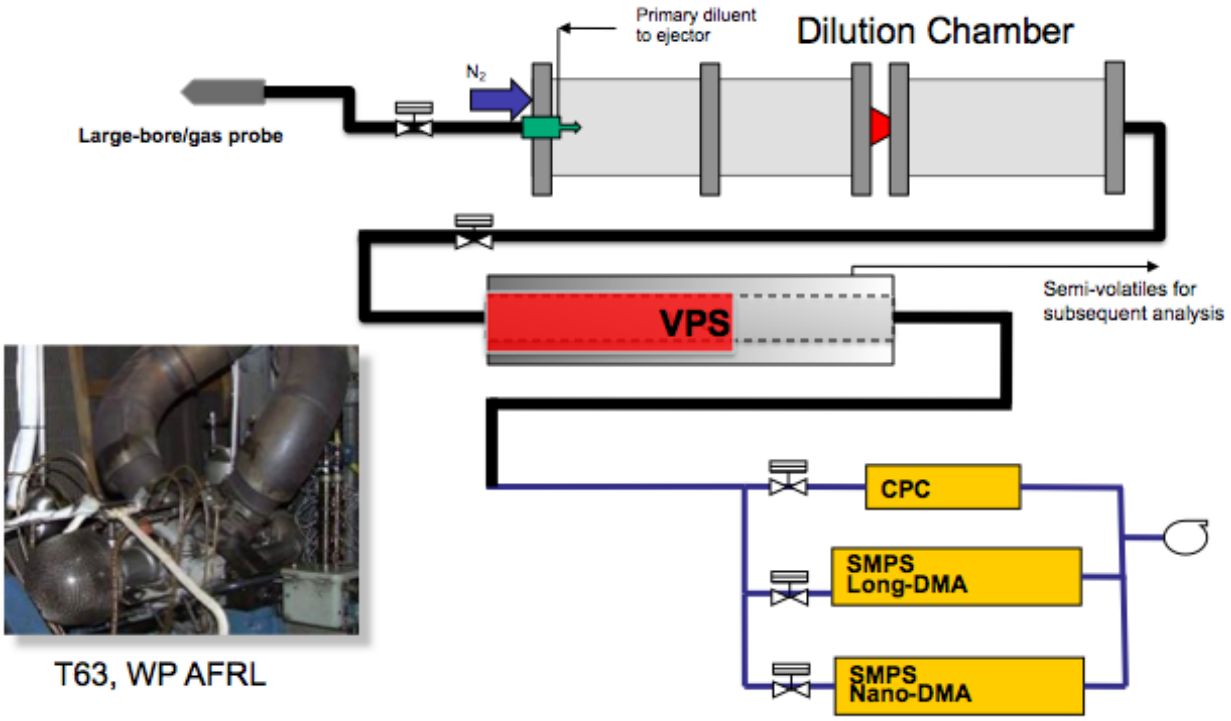

Figure 6. Illustration of reconfigurable WP1627 sampling and measurement prototype for volatile engine particles

(II.1) Design Rationale

The rationale of our design is to extract condensable particles at the engine exhaust plane using a device that we subsequently called the "dilution chamber". Thus, if the nonvolatile particle number concentration in the engine exhaust was Nnv, then after this condensing device, the total number of detectable particles will be Nnv+Nv where Nv is the volatile particles. It is important to understand that Nv will depend on the operating condition chosen by the operator. For instance, as the operating temperature is decreased and the dew point is lower, one can condense more species onto existing particles.

Then, a vaporization device (as labeled as VPS in Figure 6) is designed to remove Nv and to return the nonvolatile particles to its "dry" state such that (1) the performance of the dilution chamber (faithful measurement of Nnv) can be verified and (2) the condensable species from the dried particles can be collected and analyzed. Similar to DC, the outcome of VPS will depend on the operating condition of the device. As the vaporization temperature is increased, more species (i.e., higher molecular weight ones) will be driven out of particles. When the temperature is hot enough, a particle may be completely burned-off and the entire particle mass is transferred into gas molecules. Thus, being able to control the vaporization temperature in sequence as the VPS can, it is possible for one to develop a thermogram to allow the investigation of thermal behavior of particles, formation, and engine combustion dynamics.

It is important to remember that the mass that consists of Nv is likely to be extremely low because, for instance, the mass for a 10-nm particle is about 5×10^{-19} g assuming density of 1 g/cm^3. Given the number concentration of 10^7 cm^{-3} a concentration commonly found in engine emission for 10-nm

particles, the total mass of this 10-nm particle population would be $5x10^{-12}$ or 5 picogram. A highly sensitive gravimetric balance available today may be capable of detecting this level of concentration, but possibly not in real time. Thus, a concentrator such as a solid-phase adsorbent or an adsorption charcoal tube will have to be used and the collected species are then analyzed off-line. In a real-world application, the VPS would be most useful as a volatile particle remover (VPR) without using the built-in vapor detection function. However, as we will show in the following sections, the VPS as a VPR is more advantageous than other VPR such as thermodenuder and catalytic stripper because the VPS has high particle transmission efficiency and does not lead to measurement bias due to artificial particle formation as seen in some commercial thermodenuders (Giechaskiel et al, 2010).

(II.2) Dilution Chamber (DC)

The DC was intended to provide an unbiased sampling of aircraft engine particles. It needs to provide representative samples of nonvolatile particles such that a baseline particle concentration can be determined. The DC needs to be flexible in handling different engine thrust conditions and simple enough to enable an operator to control an experimental condition for condensing volatile particles. The DC was designed and constructed by team members at the Wright-Patterson Air Force Research Laboratory (WP AFRL). PM measurements in diesel engines are conducted using full-flow Constant Volume Sampling (CVS) systems, which dilute and condition the entire engine sample to simulate PM dilution processes in the atmosphere.

Because of the high exhaust mass flows and gas velocities, this approach is not feasible for turbine engines. For turbine engine PM sampling, the approach has been to sample a portion of the flow near the exhaust nozzle and dilute at the probe-tip with nitrogen. Although this methodology is believed to provide a good representation of the nonvolatile PM emissions, it is complex and sample dilution downstream of the engine exit is preferable as engine manufacturers can use existing gas probes and rakes. The DC in this project was designed to provide an easy and effective (i.e., low PM loss) means of diluting a hot, PM turbine engine exhaust sample collected at the exit plane in a controlled manner, while maintaining its physical characteristics.

PM samples require dilution to reduce concentrations to the range of existing aerosol instruments and to minimize losses through sampling system lines. The DC was designed to promote condensation and thus, the formation of volatile particles (simulating ambient dilution), which can then be characterized using conventional aerosol instruments. If operated properly, the DC may be used to provide a nonvolatile sample to the instruments. The DC (Figure 7) has a cylindrical design with three regions: exhaust sample injection and primary dilution zone (via an ejector and motive flow), a secondary diluent zone, and a turbulent mixing zone. Raw exhaust is extracted at the engine exit plane, drawn to the dilution chamber by exit plane, and drawn to the dilution chamber by the ejector via a 0.77 cm diameter stainless steel heated line at 150°C.

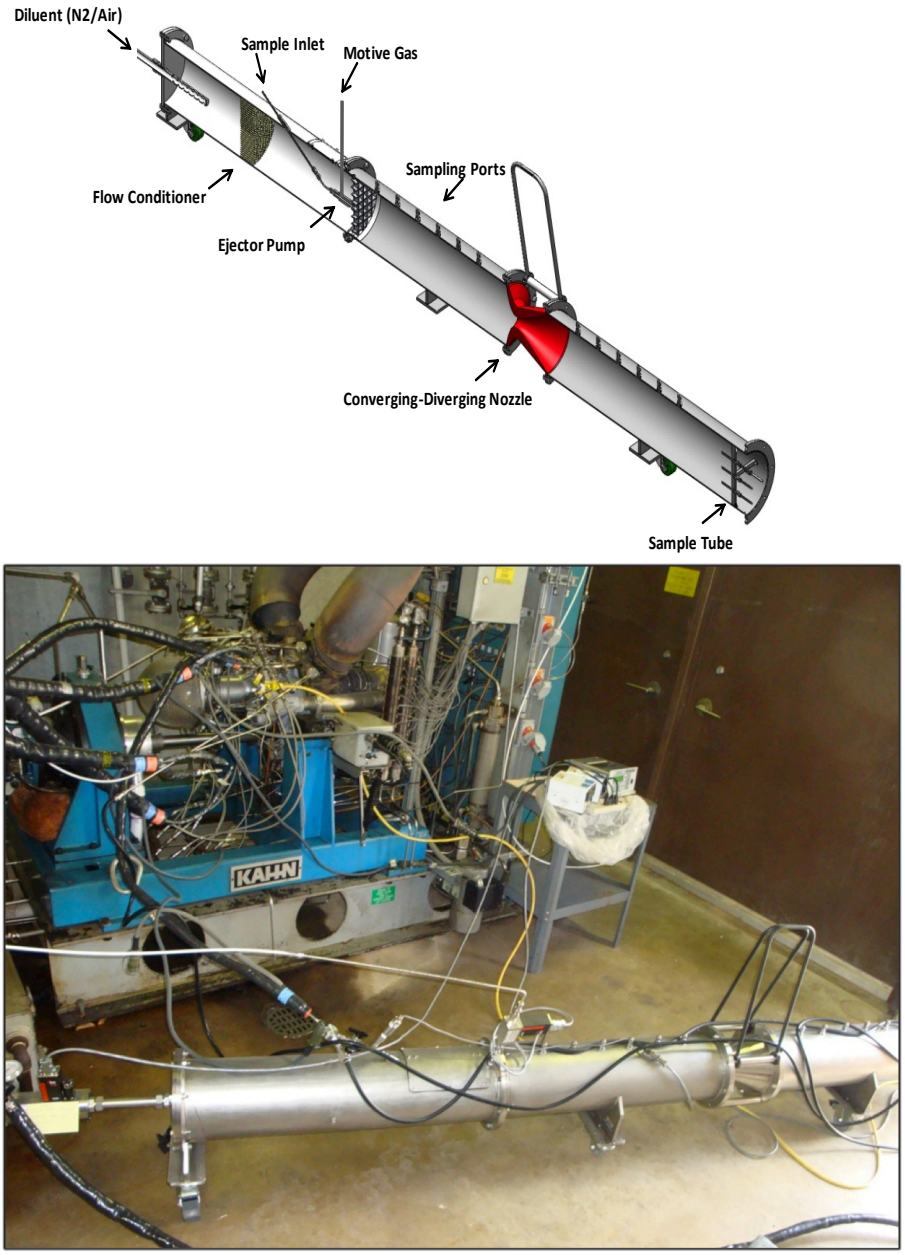

Figure 7. Computer Drawing of Dilution Chamber (a) and Implementation of DC for Sampling from T63 Engine

Compressed ambient air or dry nitrogen gas is used as the motive (driver) flow depending on experimental design. The raw sample residence times were typically 60-100 milliseconds before reaching the ejector. Low raw sample residence times and high temperatures before dilution are desirable to maintain sample integrity and reduce particle losses and agglomeration. The sample is then diluted with compressed nitrogen or ambient air drawn in the DC with a variable speed blower. The secondary diluent enters the DC and passed through a flow conditioner before mixing with the partially diluted sample from

the ejector. The mixing section downstream of the ejector is comprised of a converging/ diverging section and a homogeneous sampling zone. The DC section downstream of the ejector section is actively heated to 75°C and insulated to prevent condensation of combustion species on the DC walls.

The DC was designed based on CFD modeling using Fluent software and the turbulent RNG k-ε RANS model approach. The radial and axial exhaust profiles were used to assess the homogeneity of the conditioned gas stream. The methodology resulted in a design with a converging/diverging section to promote convective mixing of the sample and diluent streams to overcome diffusional transport limitations. The DC has an internal diameter of 0.21 m with a cylindrical inlet length of 0.80 m. The internal diameter then rapidly converges to 0.038 m followed by a gradual divergence to the original diameter over the next 0.10 m. The diluted sample extraction point is located approximately 1.10 m downstream of the converging/diverting section throat.

An axisymmetric cross-section of the DC is shown in Figure 8 with the predicted mixing characteristics for CO_2 as a function of axial and radial position for a dilution ratio of 100:1. The CFD analyses indicated that the process stream would be fully developed at the downstream sampling location. The concentration of CO_2, used as the representative trace gas for these calculations, is initially non-homogeneous through the cross-section. However, once the stream passes through the converging/diverging section (axial distance of 1.0 m), the stream is radially homogeneous at the extraction point. During engine sampling, the diluted sample is collected in the mixing zone via a 0.635 cm SS tube, and transferred to the instrumentation through an unheated stainless steel or carbon impregnated PTFE line.

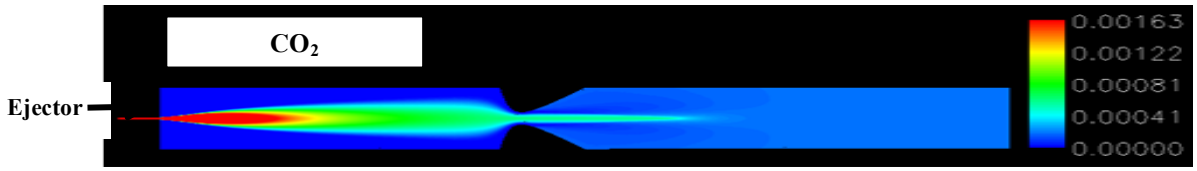

Figure 8. Axis-symmetric cross-section modeling for dilution chamber design (Dilution Ratio: 100:1)

The DC was evaluated in the laboratory to validate the CFD model and ensure a homogenous diluted sample at the extraction point. Characterization was performed using CO_2 calibration gas drawn into the ejector with nitrogen motive flows at conditions simulating engine exit pressures. Sample homogeneity was evaluated by extracting samples at different axial and radial locations of the DC while operating at different overall dilution ratios. Test results (Figure 9) validated the CFD results showing that the DC provides radially uniform CO_2 concentration profiles at relatively short distances from the ejector, even for a low dilution ratio of 20:1. This allows for sample extraction for transport to the instruments at a single location in the DC without concern of sample quality. It is expected that PM mixing characteristics will be similar to those observed during the CO_2 tests.

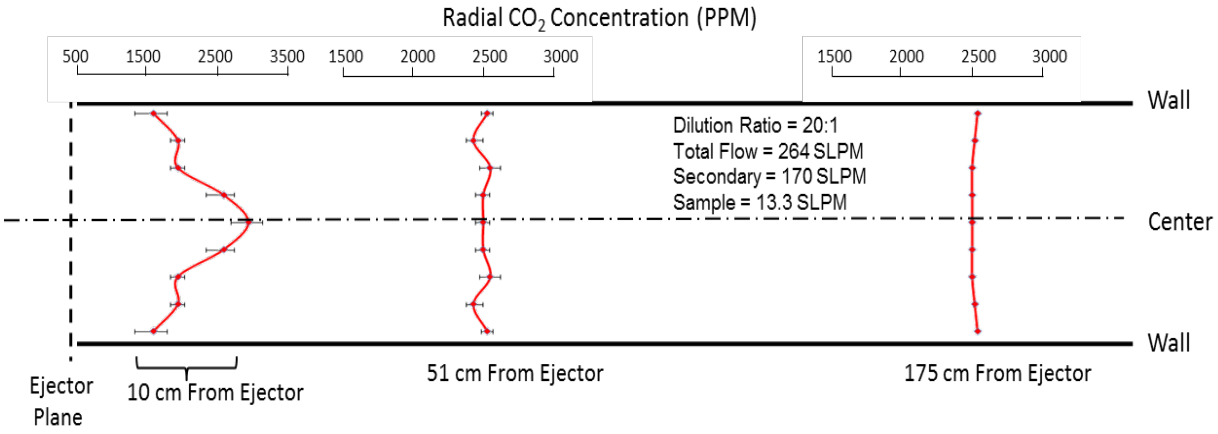

Figure 9. Measured CO2 Concentration in DC at 3 radial and axial locations

(II.3) Vapor-Particle Separator (VPS)

In contrast to current thermodenuder technology that utilize adsorption as the means of removing vapor from particles, our VPS technique applies the principle of membrane separation in a counter-flow filtration design to remove vapors and prevent re-condensation of desorbed vapor. This approach not only effectively separates vapor from particles, such that vapors are removed from the system, but also permits the collection of vapor (e.g., by canisters, solid-phase extraction cartridges, etc.) that can be subsequently analyzed for chemical speciation, which is a new capability that does not exist in current thermodenuder or any catalytic strippers. Operationally, the new approach removes the vapors before they even have a chance to condense, eliminating the need to replace the adsorbents, thus, it greatly simplifies the maintenance of the instrument.

Figure 10 shows a drawing of the main components of the VPS tested. In this design, the heating section is about 30.5 cm long (a total of 38.1 cm long of the ceramic insulation casing). The number scale at the bottom of this figure is in inches. The ceramic casing ensures a homogeneous radially uniform temperature distribution, while it also provides thermal safety protection. To ensure the safety of the instrument when operating at high temperature, outside of the ceramic casing have several additional layers of glass fiber insulation blanket. Particles entering the VPS first go through this heating section, which is followed by a section for membrane separation of nonvolatile particles from the vapors.

The double-layer metallic microporous membrane tube has an ID about 1.91 cm and 25.4 cm long. The proprietary manufacturing technology ORNL developed can make the membrane in different shapes and geometric dimensions, if it is so desired. The membrane can also be made with materials other than the stainless steel that was used here in this project. The primary layer (the layer that is the inner most in the tube) has a nominal pore size of 0.4 micrometers, and the structural support layer is about 40 microns of nominal pore size. The total thickness of the double-layer structure is about 420 micrometers. The membrane is made of 306L stainless steel granules that can resist pressure greater than 400 kPa and backpressure greater than 10 kPa. The membrane tube (on the right side in Figure 10) is connected to the heating section by a tight sealed Swagelok® union connector, which also acts as a heat sink.

The membrane tube is completely enclosed inside a stainless steel cylinder of 2.54 cm ID. There are two exit ports on the cylinder to enable the maintenance of a lower pressure region to encourage vapor

diffusion transport from inside through the membrane to the outer space between the membrane wall and the stainless steel cylinder. A gauge monitors the pressure differential across the membrane and is used to check the pressure gradient ensuring a positive transport of vapors through the membrane. Fuel vapors that are not burned will also penetrate the membrane and be evacuated. Due to the unburned fuel vapor, this becomes the main reason why it is difficult to detect the chemical species in the vapor phase on-line. However, if the chemical species is unique and not present in the fuel vapor and the analytical instrument is capable of detecting it, then the vapor port is useful for the purpose. This idea was tested during the test of using Dioctyl Phthalate (DOP) and we were able to detect the vapor-phase DOP and its thermally decomposed by-products due to that there was no other DOP source that could emit the vapor into the aerosol stream.

In addition, the exit temperature from the membrane section is generally around 50°C for a heating temperature of above 250°C, and the entrance temperature at the membrane is around 150°C. Particle measurement was done at the entrance of the membrane to verify if the decrease of temperature from 250 to 150 caused any particle formation; we have not been able to detection any. Thus, it appears there is no particle formation in that short distance of the Swagelok connector.

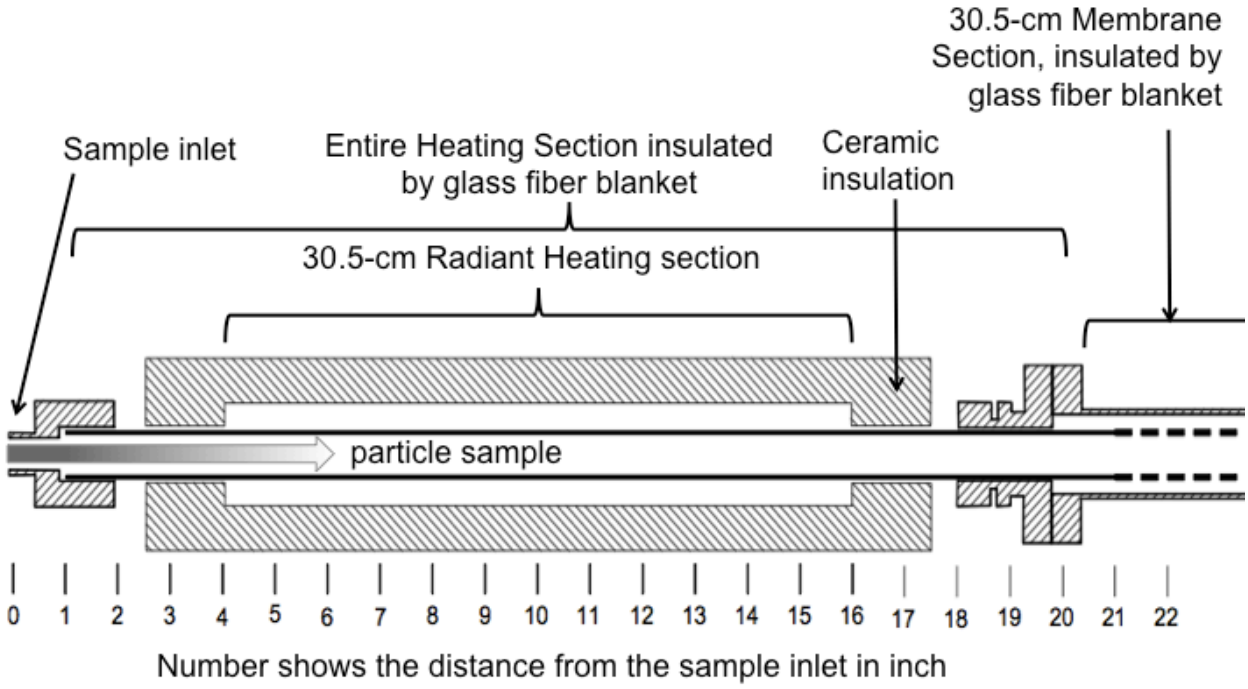

Figure 10. Computer drawing of the heating section of the VPS

The heating section of the VPS is a stainless steel 306L tube of 30.5 cm long and 1.91 cm ID. It is immersed inside of a 600W radiant heater insulated by ceramic clamp-shell casing and another thick layer of fiberglass insulation clothes on top of the casing. The heater takes less than 5 Amperes of current and control input from a PID. The axial temperature profiles for three flow rates through the VPS are displayed in Figure 11 for the set point temperature of 250°C. The shaded area in Figure 11 represents the approximate length of the active heating section (about 27.94 cm). The three temperature distributions in the axial direction are in a smooth symmetrical shape around the center where the set point temperature was monitored by a K-type thermocouple, indicating the ceramic radiant heater was performed well as compared to those reported previously.

As the sample flow through the heating section increased from 0 to 1 lpm, the peak of the distribution shifted by about 5 cm to the right as predicted from the heat transfer calculation and the peak temperature decrease also by about 1ºC. The curve shifted further to the right when the flow was increased to 2 lpm, the peak was 10 cm from where it was at 0 lpm and the peak temperature decreased to around 235 instead of 250. The heating resident time is approximately 2.6 second estimated at the flow rate of 2 lpm. This residence time is more than sufficient to completely desorb volatiles of a set temperature according to the design formula. The axial temperature profiles at a higher temperature set points are in a similar trend with airflow rate as those shown in Figure 11 for 250°C except the curve moves upward on the temperature scale.

The membrane section for vapor-particle separation that follows the heating section shown in Figure 12 is enclosed in a 5-cm diameter stainless steel tube. The inner space between the metallic membrane and inner wall of the stainless steel tube serves as the volume temporally holding the escaped vapors before they are evacuated by the extraction pump mentioned previously, which leaves no opportunity for the vapor to re-enter the membrane and condense on the particles. We measured the temperature at the location labeled "21" in Figure 10 and found it to be 150°C when the set point temperature was at 250°C and the flow rate at 2 lpm. Thus, it is unlikely that the vapors could condense back to particles at this point. The temperature at the other (i.e., the exit) end of the separation section is 50°C or less. The drawing shown in Figure 12 is a close-up view of the membrane section.

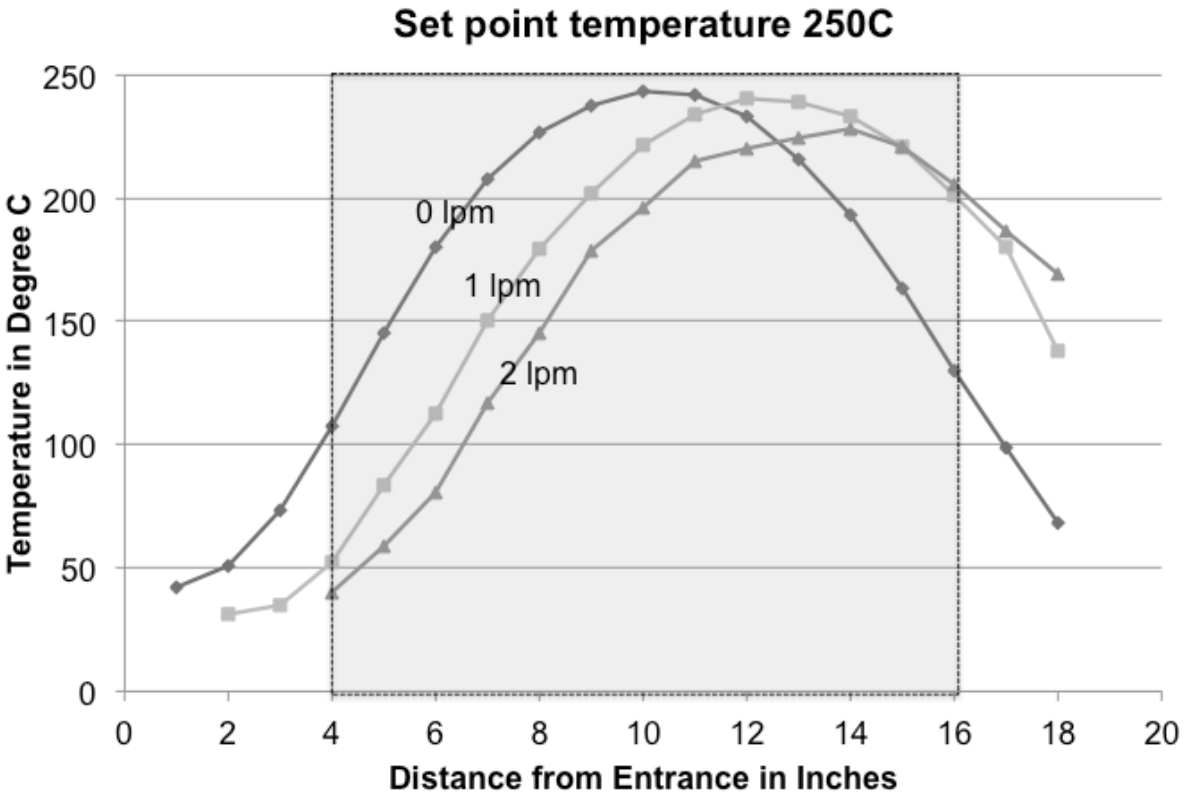

Figure 11. Axial temperature profiles of the VPS heating operation

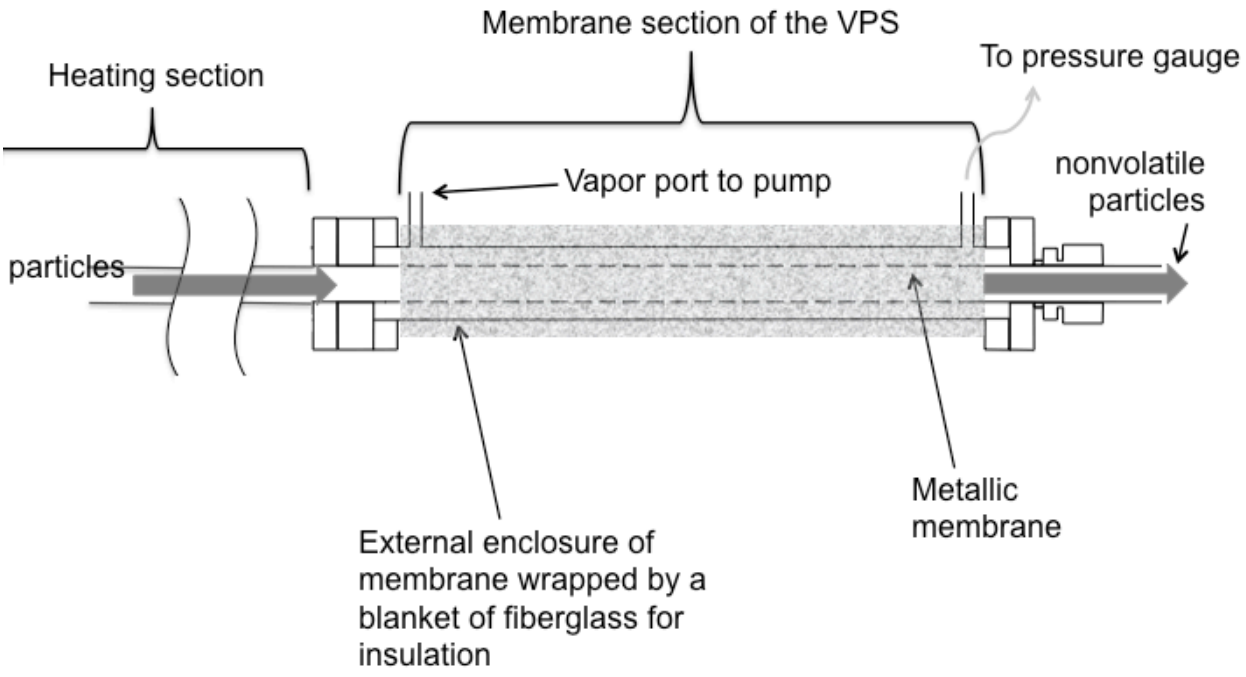

Figure 12. Computer drawing of the membrane section of the VPS showing the enclosure of the membrane tube

The scanning electron microscopic image shown in the left panel (a) of Figure 13 is an example of the surface of a metallic membrane, while the right panel 13(c) shows a drawing of the double-layer structure of the membrane. Figure 13(b) shows the dimension of one of the metallic membrane tubes tested during the research.

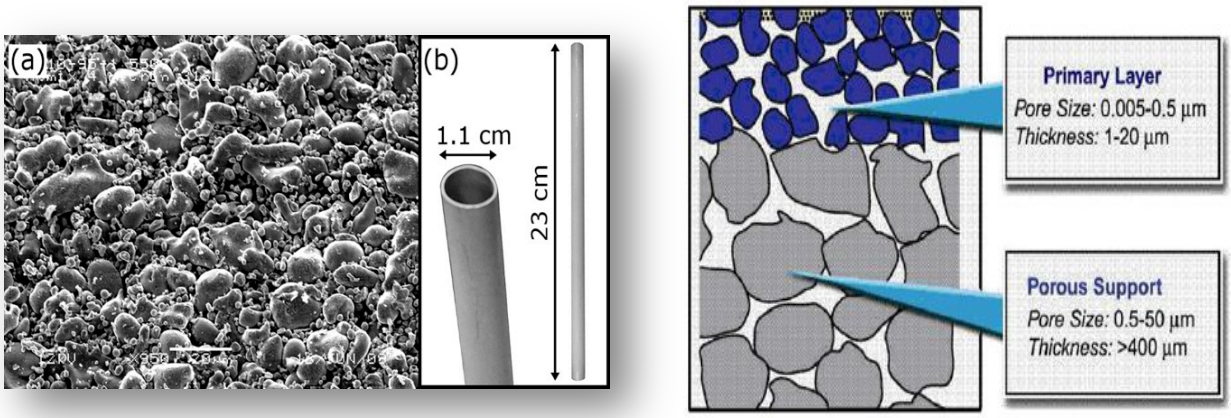

Figure 13. SEM micrograph of the membrane surface (a), dimension of a tube (b), and illustration of the double layer structure (adapted from Phelps et al., 2008)

Upon completion of the design and manufacturing of several membranes (of various properties) using the ORNL propriety technology, the VPS instrument was assembled and evaluated using synthetic particles from reagent-grade chemicals. The experiments using the pure synthetic particles were performed in the aerosol science laboratory at Oak Ridge National Laboratory (ORNL). An atomizer (see Figure 5 for the TSI 3076 atomizer, photo taken from the TSI, Inc. web site, http://www.tsi.com) was used to generate the test particles from the prepared stock solution.

The synthetic particles include sodium chloride (NaCl), ammonium sulfate $(NH_4)_2SO_4$, sucrose, and DOP. The materials including NaCl and nano-silver have vapor pressure much less than 10^{-4} mmHg at the room temperature; thus, the aerosol particles made from these materials are essentially nonvolatile. Ammonium sulfate and dioctyl phthalate are considered as semi-volatile at the room temperature, because of their vapor pressures. Sucrose is also considered as semi-volatile material, but at a higher temperature than ammonium sulfate and DOP. Nanopured water of 18 MΩ was used in the preparation of all stock solutions, except DOP, for particle generation. The NaCl stock was prepared as 0.1% w/w (weight-to-weight) solution and so was $(NH_4)_2SO_4$ and sucrose. DOP was prepared as 0.01% v/v (volume-to-volume) but the solution was 50/50 water and ethyl alcohol mixture. The stock solutions of these chemicals are stored in a refrigerator when they are not used.

In each experiment, a prepared solution was atomized (by the TSI 3076 atomizer) to generate aerosol particles for the tests. Dry HEPA-filtered air was used to drive the atomization. The generated aerosol was dried in a 30-cm linear length and 4" ID column by mixing with dry (RH < 5%) particle-free air; then the particle stream would pass through diffusion dryer. Hygrometer measurement of the dried aerosol stream shows the relative humidity in the air was less than 7%. The test aerosol particles were then used for challenging the VPS in two ways: (1) monodisperse operation by using a size selector such as the differential mobility analyzer (DMA) in the Tandem DMA operation (see Section III.2.2) or (2) polydisperse mode without use of any size selector.

Figure 14 is a photo of the interior of the VPS. The instrument box is constructed of aluminum-re-enforced panel of extremely lightweight and sturdy. The frame is built from aluminum structure. The left side of the system in the box is the heating section of a stainless steel tube heavily wrapped with insulation under which is the ceramic radiant heater. To the right side is the stainless steel enclosure of the membrane section that is also insulation wrapped. Both sections are connected by using a Swagelok union. This connector is insulated lightly. In Figure 15, on the outside of the box to the left is the control panel in black color and the right side is the differential pressure gauge designed to monitor the trans-membrane pressure. Both controls are clearly labeled. The size of this VPS instrument can be reduced in the near future, if it is needed, since there are plenty of empty spaces inside the box. The aerosol flow is driven by vacuum pump placed outside the instrument box not shown in the figure.

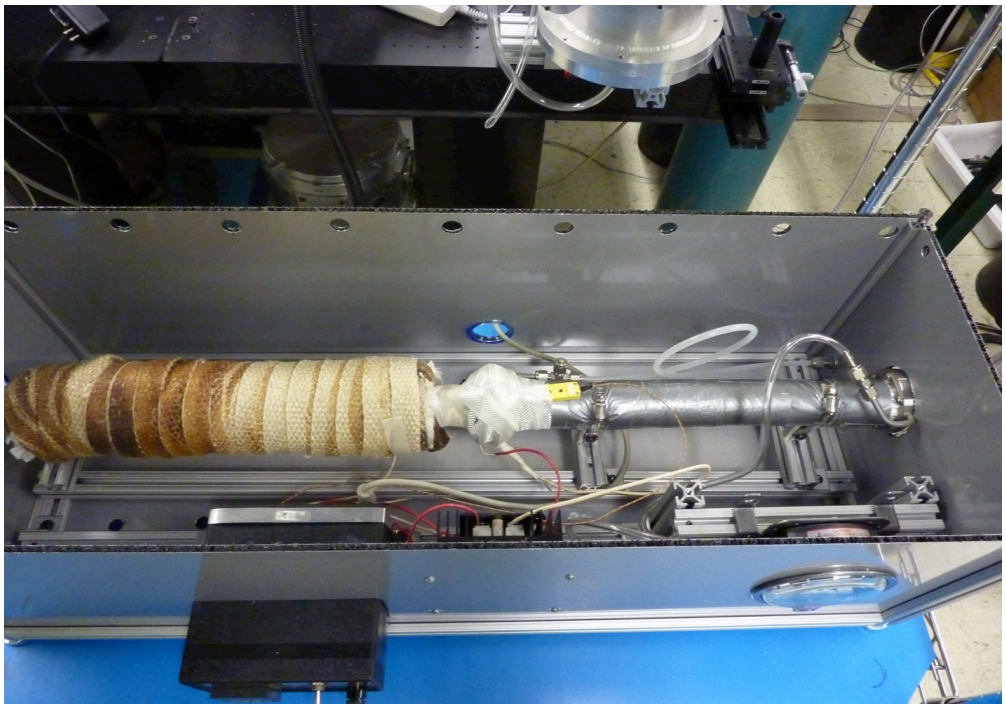

Figure 14. Photo of the interior of the VPS.

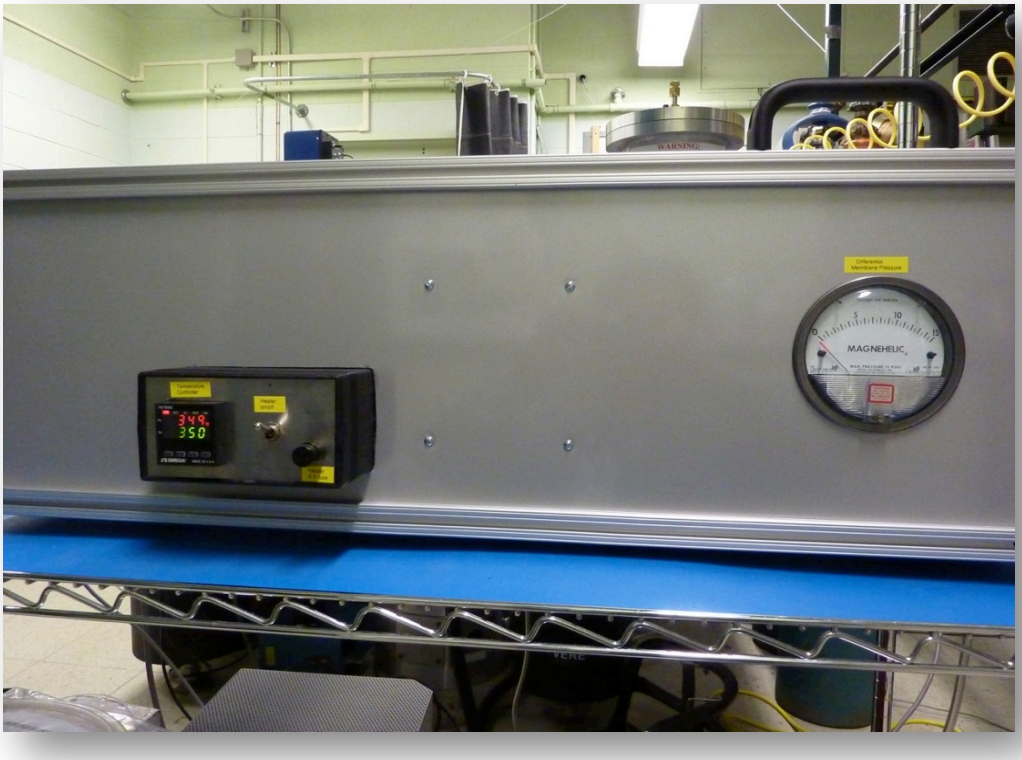

Figure 15. Photo of the exterior of the VPS

(III) RESULTS AND DISCUSSION

The data presented in this chapter are the test results conducted throughout the project. Most of the tests have been performed in highly controlled laboratory conditions during Phase 1 stage where impacts or disturbances caused by uncontrollable environmental factors were minimized. Toward the end of second and third years, tests were also performed on a diesel engine or an aircraft engine where controls over the property of particles were less stringent than in the laboratory condition due to the scale and complexity involved in engine experiments. Finally, limited field tests of the instruments were also conducted in collaboration with other aircraft emissions campaign which environmental conditions were uncontrollable and could affect the results more than that in the lab conditions.

(III.1) Dilution Chamber

We had reported in Section II.2 on the confirmation of engineering design by experimental data from carbon dioxide showing the dilution chamber (DC) performed the dilution tasks "as expected" from the CFD prediction. The DC was evaluated primarily in the engine lab at the Wright-Patterson AFRL where a T63 class of turboprop engine was available or in field conditions in two "piggy-back" alternative fuel turbine engine emissions tests during the last several years. Although valuable field data were collected and experience gained on the field operation, limited conditions were examined, as these field tests were not focused on the evaluation of the DC performance. The capability of the DC to condense exhaust particles was not investigated in this project due to the limitation of resources, although the capability was designed in the DC. This capability will be tested in the near future, if resources are available to the team members.

(III.1.1) C-17 (F117-PW-100 Engine) Tests

C-17 emissions tests were performed in August 2010 to support the certification of the aircraft on 50/50 blends of JP-8 and Hydroprocessed Esters and Fatty Acid (HEFA) fuel (Corporan et al., 2011). For these evaluations, emissions were measured at engine powers ranging from 4 to ~63% of max thrust. PM emissions were sampled and quantified using both probe-tip and DC dilution. For the DC, the raw engine exhaust sample was extracted through a gas probe installed on a probe rake located 42 cm from the engine exhaust. The sample was drawn through a 2.4 m long, 0.77 cm diameter heated line (150°C) using a nitrogen-driven (motive flow) ejector pump. The sample was further diluted with nitrogen gas (secondary flow) to obtain the desired overall dilution. The sampling setup during the C-17 test is shown in Figure 16. The 3 white boxes at the base of the sampling rake are water tank each contains about 300 gallons of water used to weigh the rake against the engine thrust during the test. The sampling probes include gas and particulate probes are located at the top of the rake. The dilution chamber is the metallic stainless steel instrument placed on the ground to the lower half of the photo in Figure 16.

Figure 16. Photo of the sampling rake setup for C-17 emissions test. The probes are located at the top of the rake.

Since ambient air was not used as a diluent, minimal physical/chemical transformations of the PM emissions were expected. The motive and secondary dilution flows provided total dilution ratios of 19 to 50:1. The diluted sample was collected at a single point near the center of the DC at 1.10 m from the converging/diverging section and transported to dedicated SMPS and CPC instruments via unheated 23 m long, 0.77 cm I.D. stainless steel tubing.

Test results of average particle number emission indices (EI_n) and particle size distributions using the two dilution methods are shown in Figure 17. Excellent agreement in EI_n and size distribution profiles between probe-tip and N_2-diluted dilution chamber sampling are observed throughout the test conditions evaluated. **These results suggest that particle integrity is conserved in the DC and that it may be a valid tool for the characterization of mostly nonvolatile PM without the complications associated with dilution at the probe-tip.** Due to the dry/inert nature of the dilution N_2, there was negligible nucleation of new particles from sulfur and organic species. Dilution of the sample using atmospheric air in the DC is expected to promote the condensation of these species and the formation of PM nuclei as has been observed in far field measurements (Wey et al., 2007; Bulzan et al., 2010).

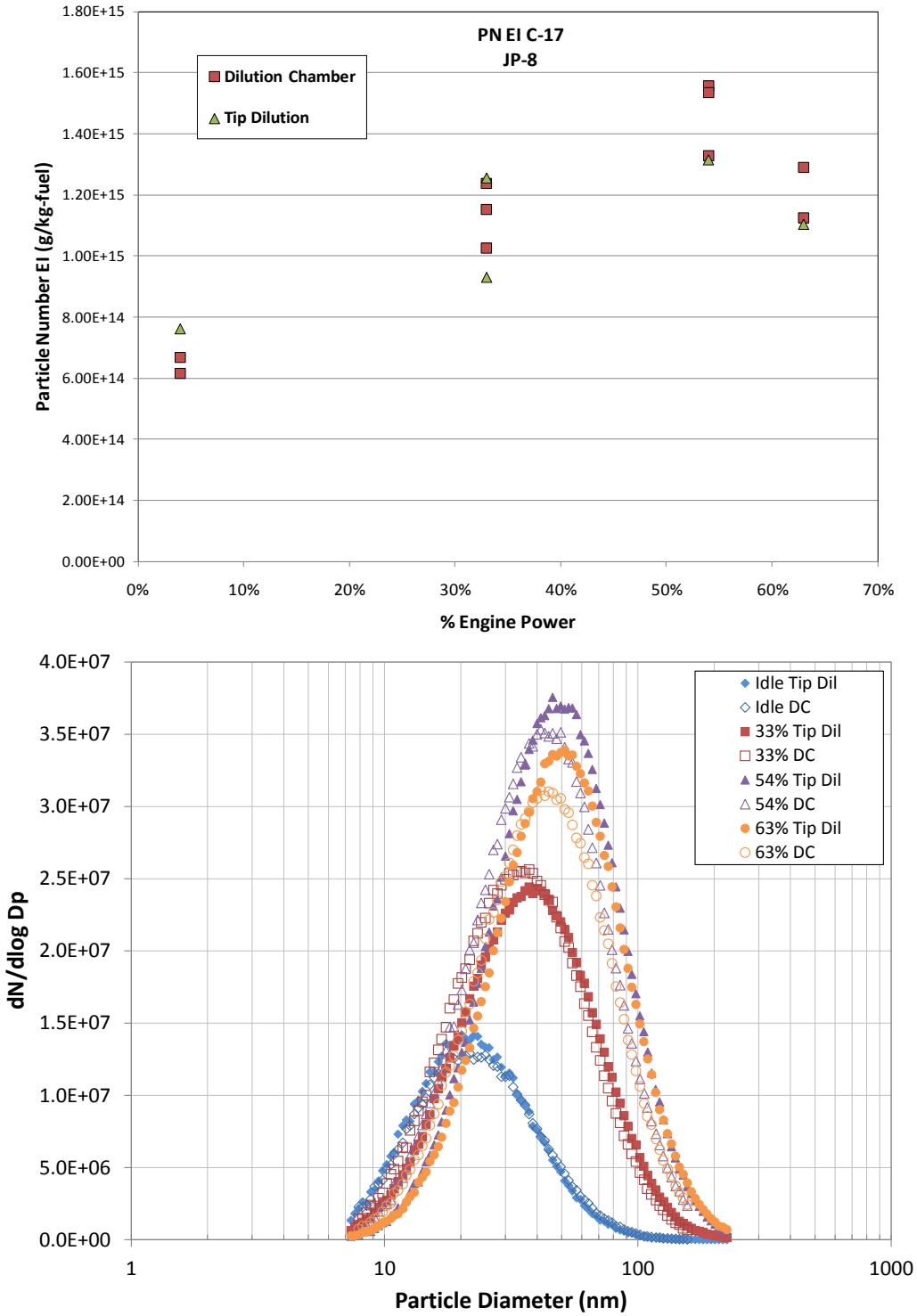

Figure 17. Average PM measurement in F117 engine at several power settings for probe-tip and N2-diluted DC: (a) upper panel the particle number EI, and (b) lower panel the particle size distribution

(III.1.2) DC-8 (CFM56-2 Engine) Tests

A CFM56-2 engine was tested under the NASA AAFEX II program to study engine emissions burning several alternative fuels. Similar to the C-17 tests, PM samples were collected at the engine exit plane and diluted at the probe-tip and in the DC. In addition, samples were obtained at approximately 30 meters downstream of the engine exit plane. For the DC, the PM samples were drawn with the ejector using N_2 as the motive gas and further diluted with atmospheric air in the secondary path. Particle size distributions and particle numbers (EI_n) for engine PM collected using the three dilution schemes are shown in the lower panel of Figure 18.

For several power settings, the samples diluted in the DC and at 30 m downstream consistently yielded significantly higher particle numbers than for probe tip dilution as shown in the upper panel of Figure 18, which are attributed to the condensation of volatile species. The difference between tip (1 m) and downstream (30 m) dilution was more pronounced at lower engine power due to the larger concentration of organic species prone to condensation to nucleate into new particles and/or condensation sites for sulfuric acid aerosols. A reasonably good agreement was observed for the DC and 30 m size distributions; however, the nucleation mode observed at 30 m with JP-8 was not fully replicated in the DC. This may be due the fact that the motive gas in the ejector was nitrogen and not atmospheric air, which may have limited gas-to-particle transformations.

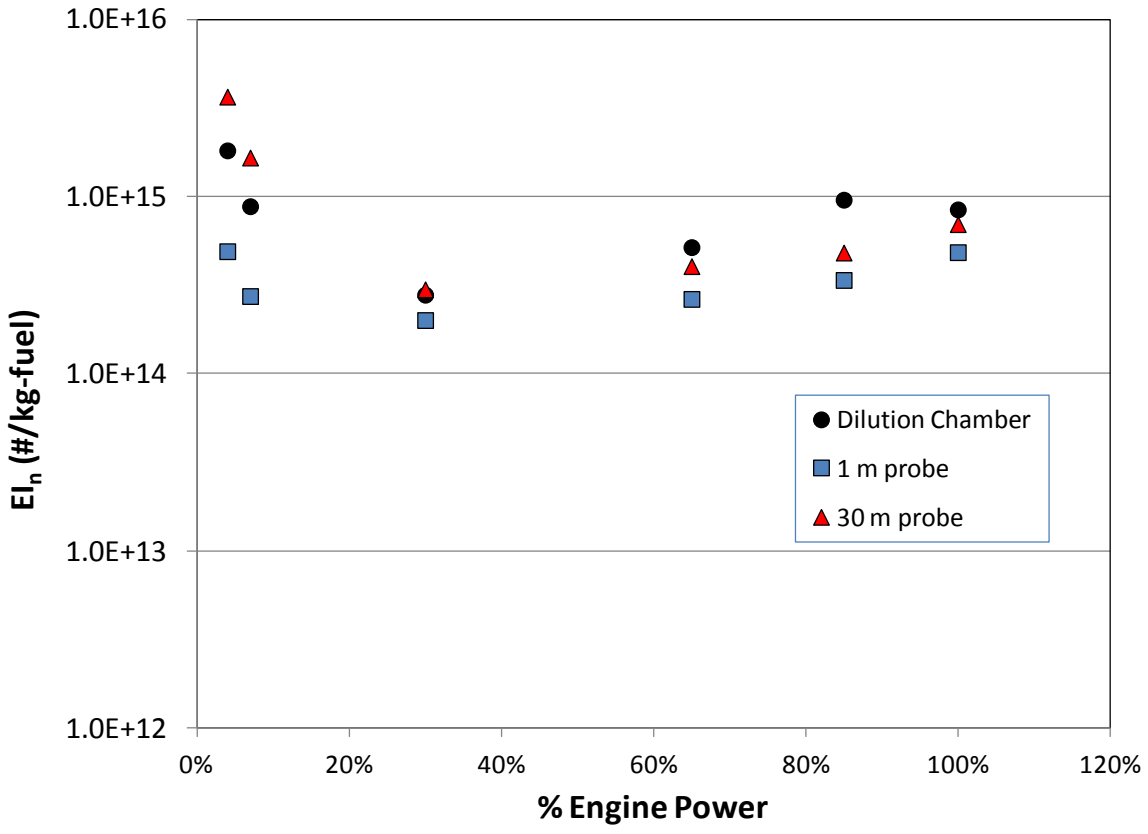

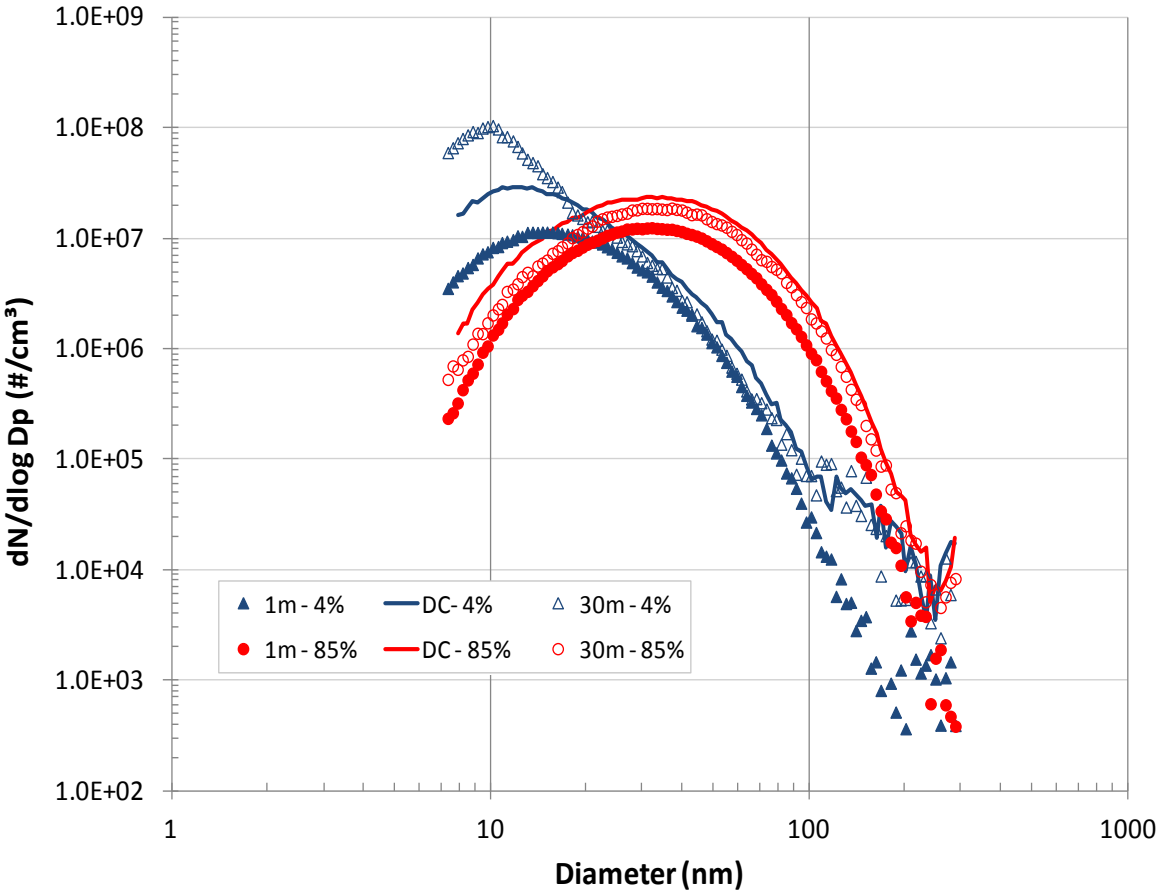

Figure 18. Impacts of PM dilution techniques on particle number EI and size distribution for CFM56-2 engine during the NASA-sponsored AAFEX II tests JP-8

(III.2) Vapor-Particle Separator

(III.2.1) Tests of VPS Using Laboratory-Generated Particles

To evaluate the performance of the VPS, a number of criteria were established. The main index of success for the VPS is its ability to completely vaporize particles at a designed temperature; in other words, the particle count or number concentration at the exit of the VPS will be significantly lower than that at the inlet and no artificial particle formation can be detected as the result of volatile particle removal. This is exactly the purpose for a **v**olatile **p**article **r**emover (VPR) that the aircraft emissions community is interested. In our design, we would like to have high particle penetration efficiency through the VPS across the entire particle size spectrum of interest to engine-emission measurement. The other criteria of the design of VPS involve the ability to extract vapor species and to enable analytical measurement of the extracted vapor species. In other words, the VPS was expected to be more than just a VPR, it is to be an instrument that can yield quantitative data for improving understanding of aerosol volatility. We will report those accomplishments in this and following sections.

(III.2.1.1) Particle Penetration Efficiency

To evaluate the particle penetration performance of the VPS instrument, we established an experimental setup as shown in Figure 17. An atomizer (TSI Model 3076) was used to generate polydisperse test particles using building supply air. The building-supply air was passed through a HEPA filter to create particle-free air that was used to drive the atomization. The particles enter either the VPS or a stainless steel bypass tube (see Figure 19) that is used as the reference in the calculation of particle transmission efficiency through the VPS. The bypass tube is dimensionally identical to that of the VPS with the exception that the tube wall is solid and has no membrane.

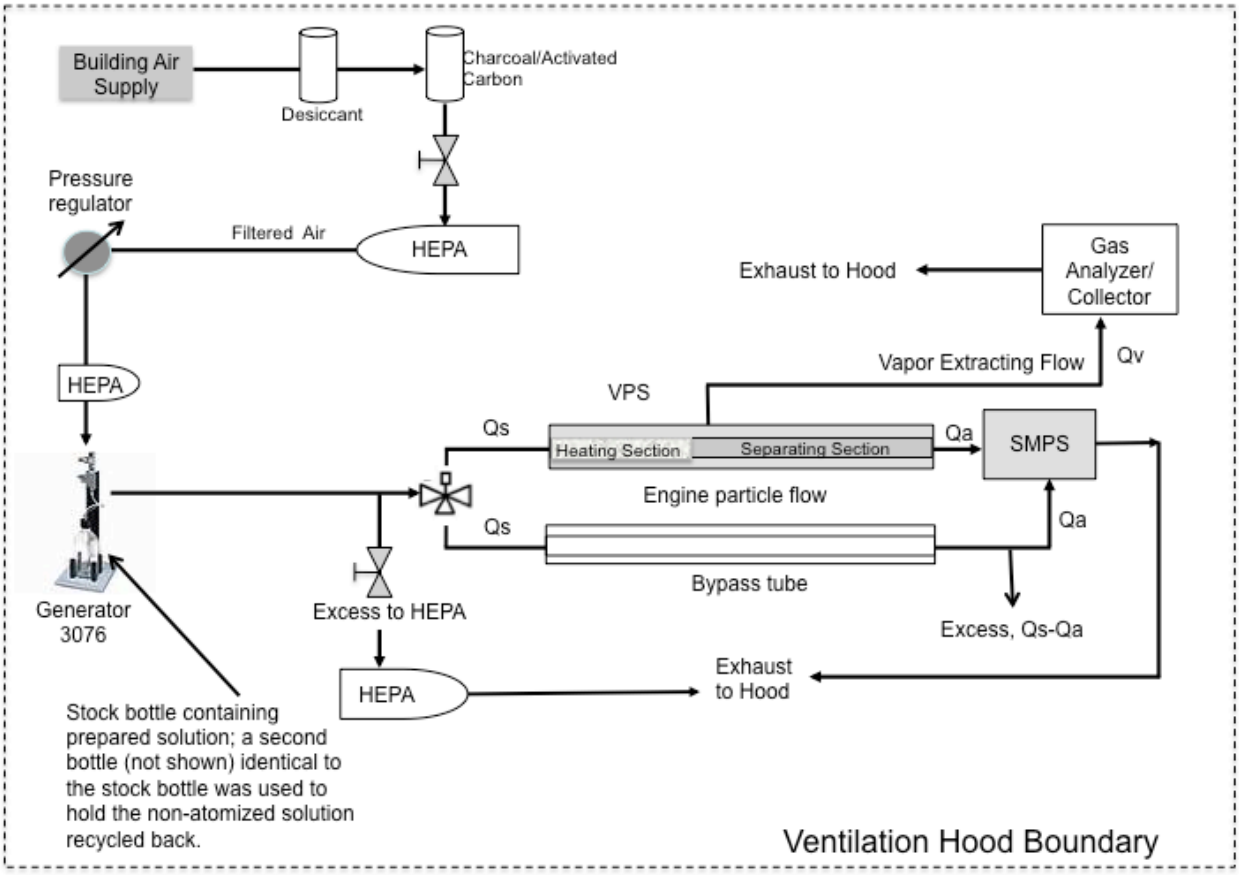

Figure 19. Experimental setup for VPS evaluation using synthetic particles in laboratory conditions

The sampling flow rate (Qs in Figure 17) through the VPS was operated at 2.0 lpm. Off the total of 2.0 lpm, 1.5 lpm was maintained to flow through the membrane section where there was 0.5 lpm (Qa) sampled by a Scanning Mobility Particle Sizer (SMPS, TSI Model 3096N) equipped with a nano-DMA (TSI Model 3085) and UCPC (TSI Model 3025A) for measurement of the particle size distribution. The rest of the sample of 1.0 lpm was unused. In the future test, this 1.0 lpm can be used by other instrumentation or applications. Vapor desorbed from particles or in the unburned fuel was removed by using a small pump operated at a volumetric rate Qv of 0.5 lpm. This vapor flow is in the normal direction to the flow streamline and is crossing through the metallic membrane. Pumping of vapors is not a required operation as this configuration is similar to the crossflow filtration in which vapor or filtrate would permeate through the membrane, due to higher diffusivity of vapor molecules than that of particles,

while the thermally dried particles would flow in parallel to the surface of the membrane. The radial velocity of the flow is insignificant compared to the axial flow velocity in this configuration, and CFD simulation using DOE MFIX model supports the experimental data.

In summary, the metallic membrane in the VPS configuration acts as an effective barrier to particles, preventing loss of particles through the membrane in the crossflow design, which preserves the true total particle count exiting the VPS to a particle instrument such as SMPS. Even small particles deposited on the surface of the membrane through, say, diffusion would be dislodged by flow sheer since the axial velocity is substantially larger than the radial one as discussed earlier.

The performance of the VPS, its particle transmission efficiency, is shown in Figure 20. The data of the Bypass are overlaying the data of the VPS showing insignificant differences in the particle number concentration (the Y-axis) across the entire particle size spectrum (the X-axis) from approximately 6 to 250nm. The bypass concentration appears to be slightly higher at the lower size (the left end) than that of the VPS, but the difference is minute.

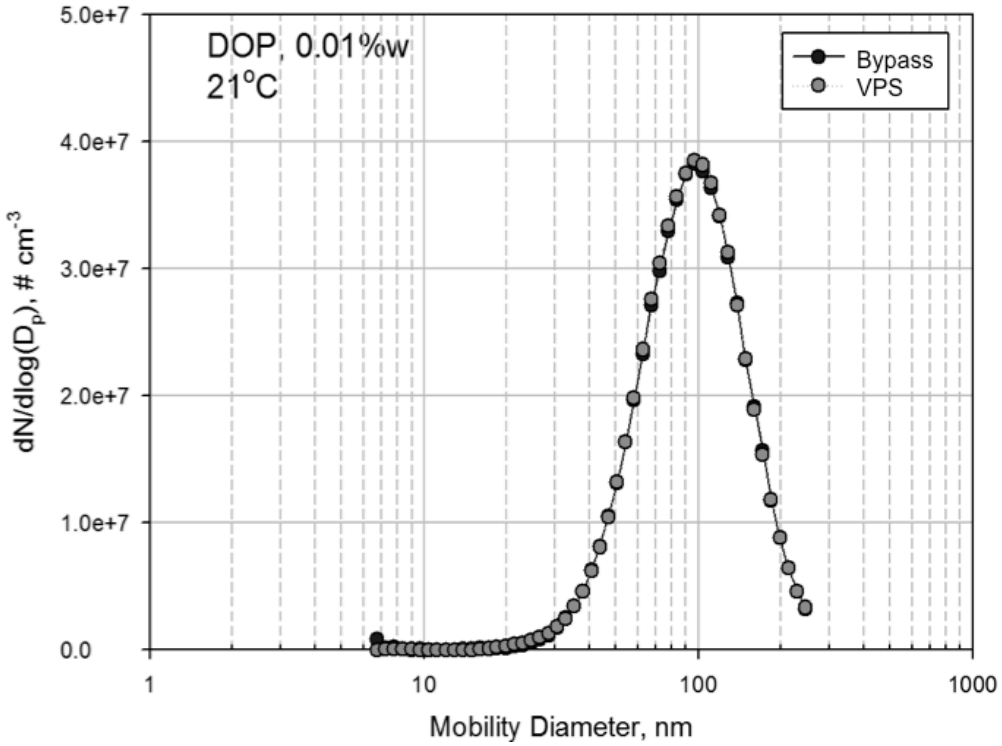

Figure 20. Size distribution for DOP particles through the by-pass and VPS. Two curves virtually overlapping each other.

Many aircraft emitted particles are in the electrical mobility diameter size range of 100nm or less. Loss of such particles is known to be a serious issue for particle measurement in the community, whether the particles are volatile or nonvolatile. Particles as small as the engine particles do not have significant inertia to be affected by aerodynamic forces (e.g., impaction and interception). However, diffusion force plays a significant role in the transport of particles. Other loss mechanisms for engine particles in a sampling tube are primarily diffusion, electrostatic, and thermophoretic. As the membrane is made of stainless steel, a conductive metal, the accumulation of static charges is negligible to cause significant

loss through the electrostatic effect. The diffusion and thermophoretic effects are two drivers of major particle loss, if any, in the VPS.

The microporous structure of the membrane appears to have no effects on particle loss in the membrane section as compared to a solid wall tube (see Figure 20) called the “by-pass”. The transmission data obtained from the by-pass is used in comparing with any other sampling configuration of the same geometry (i.e., the length, inner diameter, flow entrance and exit angles). In this case, the geometry of the membrane tube is identical to the by-pass. The results indicate a very high transmission efficiency of the VPS across a wide particle size range from a few nanometers to a couple of hundred nanometers. Again, this is the size range of most aircraft emission particles; thus, the results are encouraging.

Particle transmission is an important parameter assessing the instrument performance; an ideal particle instrument would have a 100% transmission with no loss of particles in the instrument. The test results displayed in Figure 20 show that the particle transmission efficiency of DOP particles is virtually identical to that of the bypass for all materials tested at the room temperature (no heating applied). In other words, the loss of particle in the VPS is miniscule; there was practically no loss of particles in the VPS in the size range the SMPS measured. Interestingly, similar test results have been found at the room temperature using particles created from a number of materials that include sodium chloride, sucrose, nickel chloride, and ammonium sulfate, which all showed that the transmission loss through the VPS was minimum (less than 1%). This is an impressive particle transmission efficiency as compared to those found in current commercial devices. The results also indicate the transmission is independent of material property of the particles sampled.

One question is that if the VPS can maintain such high particle transmission efficiency at an elevated temperature, since diffusion and thermophoretic transport are all temperature dependent. This question does not have a simple solution because the higher the temperature, the higher particle and gas diffusion coefficients and therefore the higher potential for diffusional loss. However, volatile particles, by definition, will be also lost through mass transfer from particulate phase to gas when thermal energy is applied. Thus, this would make it extremely difficult experimentally, if not impossible, to resolve the synergistic thermal effect on diffusion and vaporization when investigating particle transmission at high temperature. The diffusion coefficient of particles as a function of temperature is strongly dependent on the particle size (Rudyak et al., 2009). However, the transport distance between collision is the square root of the diffusion coefficient at a given transport time. Therefore, it seems unlikely that increasing the heating temperature from room temperature around 293K to even 650K would cause a substantial particle loss in the heating section through the diffusional mechanism. We addressed this issue systematically in the following sections using both nonvolatile and volatile particles.

(III.2.2) Effects of Heating Temperature on Particles

To investigate the true transmission and removal efficacy of the VPS in performing vapor-particle separation, it is convenient to use a monodisperse volatile particle than a polydisperse one. Monodisperse particles are those that have only one size in theory. In practice, if the geometric standard deviation of a particle size distribution less than or equal to 1.2, the size distribution is consider monodisperse, assuming the size distribution follows a lognormal distribution. There are many techniques to generate monodisperse particles. Electrospray technique is one of them (Chen et al., 1995; Cheng et al., 2004; Park et al., 2008). Tandem differential mobility analysis (TDMA) was demonstrated for the production of monodisperse particles (Liu et al., 1978; Rader and McMurry, 1986; Park et al., 2008; Cheng and Allman, 2011) of equivalent mobility diameter and the technique was adapted in this work. In our TDMA setup, a nano-DMA (Chen et al., 1998) was used as the size selector to extract particles from the broadband atomizer-generated particle population. Tandem DMA setup requires two electrostatic classifiers; one is used as the size selector for generation of monodisperse particles, while the other is coupled to a particle

counter such as UCPC to generate the size distribution for verification of the generated monodisperse population. An aerosol conditioner that could modify the property of the monodisperse particles is placed in between the first DMA and the second DMA, when a precision study on the particle properties in response to modification is required. For example, the conditioner can be a humidifying-dehumidifying device to enable one to study the effect of humidity on particles. In other example, a conditioner can be a vapor deposition chamber for studying the effects of coating on various behavior of coated aerosol particles one size at a time. In our case, the conditioner is the VPS that is used to enable the study of thermal effects on particles. Figure 21 shows the TDMA setup for studying the effect of temperature on monodisperse particle volatility obtained by the VPS in this project.

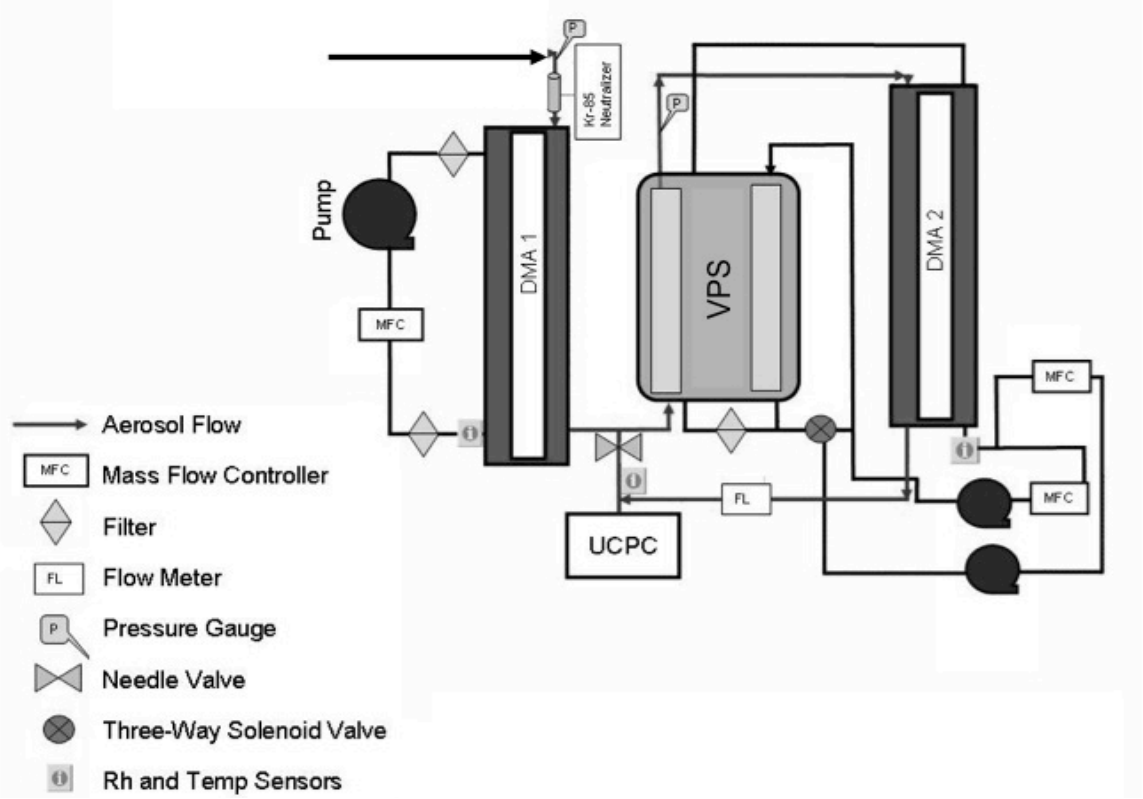

Figure 21. Setup of Tandem DMA in generating monodisperse particles for challenging VPS

Once monodisperse particles are produced, by the DMA (or called DMA1 hereafter), they are flown into the VPS where the particles are first treated thermally in the Heating Section of the VPS. The vapor-particle separation occurs at the next membrane section. Upon exiting the particle port of the VPS, the number-based size distribution is measured by a SMPS that is equipped with a long DMA and an UCPC, while the vapors leaving through the vapor port of the VPS across the membrane are collected by either charcoal or solid phase adsorption. The vapor could also be sampled directly into a detector such as a proton-transfer reaction mass spectrometer, a Fourier-transform infrared spectrometer, or other type of detector capable of on-line measurement. We found this ability is useful for study where molecular signal from particle is strong, but may not be as useful in a complex mixture like engine exhaust due to the confounding background.

(III.2.2.1) Effect of Temperature on Nonvolatile Particle Population

Sodium chloride (NaCl) is considered nonvolatile in the temperature range of 21 to 400°C. The melting point of NaCl is 801°C (1074K) and the boiling point is 1413°C (1686K) (CRC Handbook, 2009). The vapor pressure is on the order of 10^{-16} mmHg in the temperature range of the tests (NIST). There was no significant residual material in the NaCl solution that could be combined to produce the particles; thus, the contamination was ignored. Before the experiment, we did not expect NaCl particles would be vaporized.

The particle size distributions reflecting the thermal behavior of the monodisperse NaCl particles of three selected sizes (17, 28, and 55 nm) are shown in Figure 22a, b, and c. The geometric standard deviation (σ_g) of each of the selected particle sizes is less than 1.1 indicating the selected particles are all practically one size. Furthermore, there were no doubly or triply charged particles as shown in the three figures indicating high precision measurements, since the particles were fully neutralized.

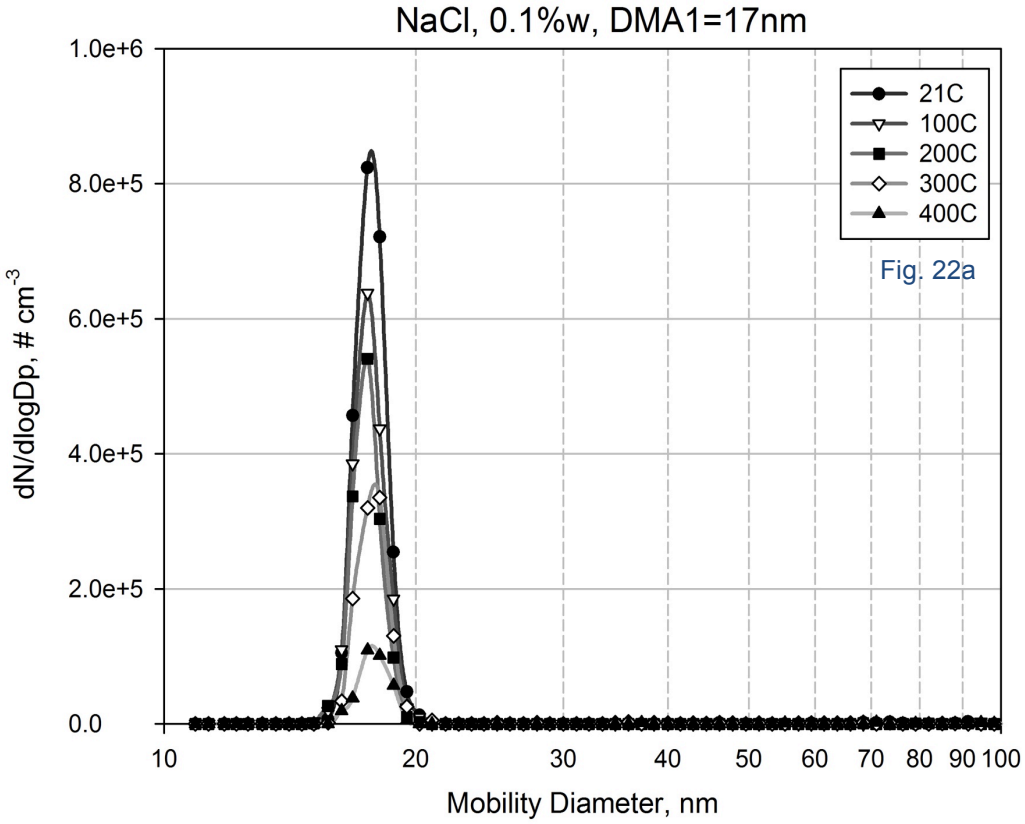

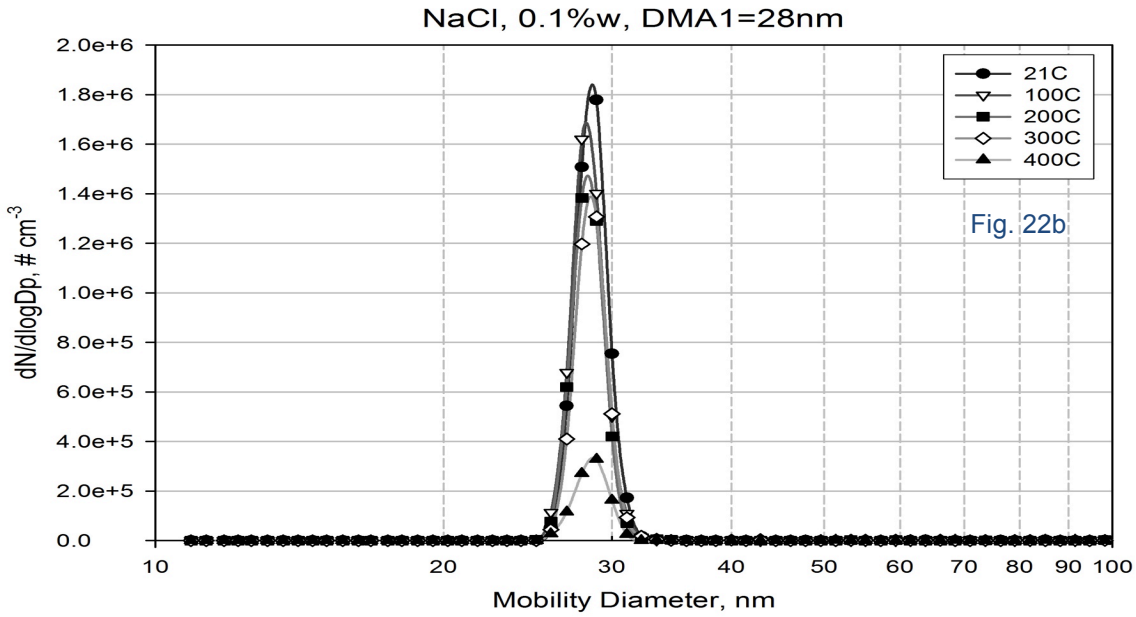

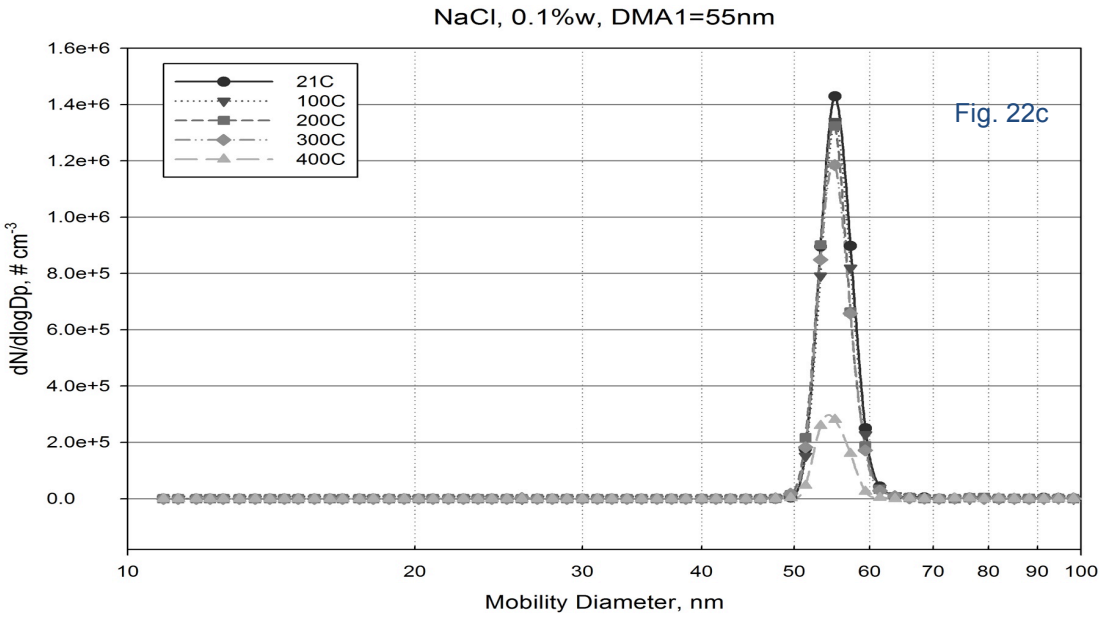

Figure 22. Size distribution of monodisperse NaCl particles in response to temperature variation in VPS

In Figure 22a for incoming 17nm, as the heating temperature (T) increased from 21ºC (the room temperature) to 100ºC, the peak mobility diameter remains unchanged. The peak height at 17 nm was

reduced by 25%, however, as T increased from 21 to 100ºC. Remember that NaCl is nonvolatile under these two temperature conditions. Loss of the 17-nm NaCl particles could be due to (1) diffusional loss of particles to the heating tube wall and or (2) vaporization caused by the heat.

Did temperature-enhanced diffusional transfer of particles to the wall of the VPS heating tube cause the loss of particles? If the membrane were capturing of NaCl particles, we should be able to detect the increase in solution conductivity if we washed the membrane. In a separate test, we used a conductivity meter (VWR Scientific Model 2052) to measure the change of conductivity on the rinsed solution and found the conductivity remained constant indicating there was no detectable amount of salt (i.e., NaCl) deposited on the wall in an experiment. We concluded that it is unlikely loss of NaCl particles to the instrument wall would have caused the greater than 25% loss of particles as the heating temperature increased from 21 to 100ºC. The particle count decreases in the results shown in Figure 22a was because of the thermal effects. The volatilization of the 17-nm NaCl particles appears to occur at a much lower temperature than expected based on the melting (801ºC) and boiling temperatures (1401 ºC) of NaCl salt grains.

As the temperature increased further from 100 to 200, 300 and 400°C, the peak size location of NaCl remained stationary at approximately 17 nm but the peak height decreased further as the heating temperature increases indicating progressively more NaCl particles vaporized as the temperature increased. The decrease in the peak height appears to accelerate from 200 to 300°C and to 400°C as compared to those at the lower temperature. The thermal behavior appears to be consistent with that described that atoms are located at the surface of nanoparticles and escaped from the main crystal structure much easier than those from a larger one, which led to a dramatically lower melting point for nano-NaCl particles. The thermal behavior of the 28- (Figure 22b) and 55-nm (Figure 22c) NaCl particles at each of the temperatures appears to be similar to that of the 17-nm particles. The stepwise change of particle number concentration at the selected 28-nm or 55-nm peak is milder in the temperature range from 21 to 300°C than that for the 17-nm particles supporting the hypothesis that 17-nm particles could be vaporized easier than larger ones. The rate of material or particle loss accelerated at the temperature from 300 to 400°C. Thus, for nonvolatile NaCl particles, increase of the heating temperature to a sufficiently high level would completely vaporize small particles in the VPS causing significant reduction in the number of particles as reflected in the SMPS spectra. This reduction is much higher than that caused by diffusional loss and the single driving mechanism of this particle number reduction is the thermal effect.

The results also raise a question regarding the operationally defined temperature for volatile engine particles, because as the nonvolatile NaCl particles could be volatilized at the lower temperature. Since the VPS allows one to operate on evacuation of NaCl vapor through the membrane (as did in this study), it reduces the potential for forming new particles in the core flow. As a result, the peak location (i.e., the size) of the monodisperse NaCl particle population did not change even in different heating temperatures, but the number of particles did get reduced as a result of the thermal vaporization.

(III.2.2.2) Thermal Effect on Volatile Particle Population

When the VPS was applied to monodisperse DOP particles, the particle population dynamics in response to the addition of thermal energy was more complex than that of NaCl. The melting point of DOP is -50°C (223K) and boiling point is 385°C (658K). The vapor pressure at the room temperature (21°C) is on the order of $6x10^{-8}$ mmHg, $5x10^{-6}$ at 50°C and $1.4x10^{-3}$at 100°C based on the Antoine equation (NIST). The results for DOP are plotted in Figure 23a, b, and c for the three selected particle sizes of 30, 50 and 80nm, respectively. The thermal behavior of the 30-nm DOP particles is shown in Figure 23a. The peak size was actually slightly off from the labeled 30 nm, but that labeling should not affect the change pattern discussed in this report.

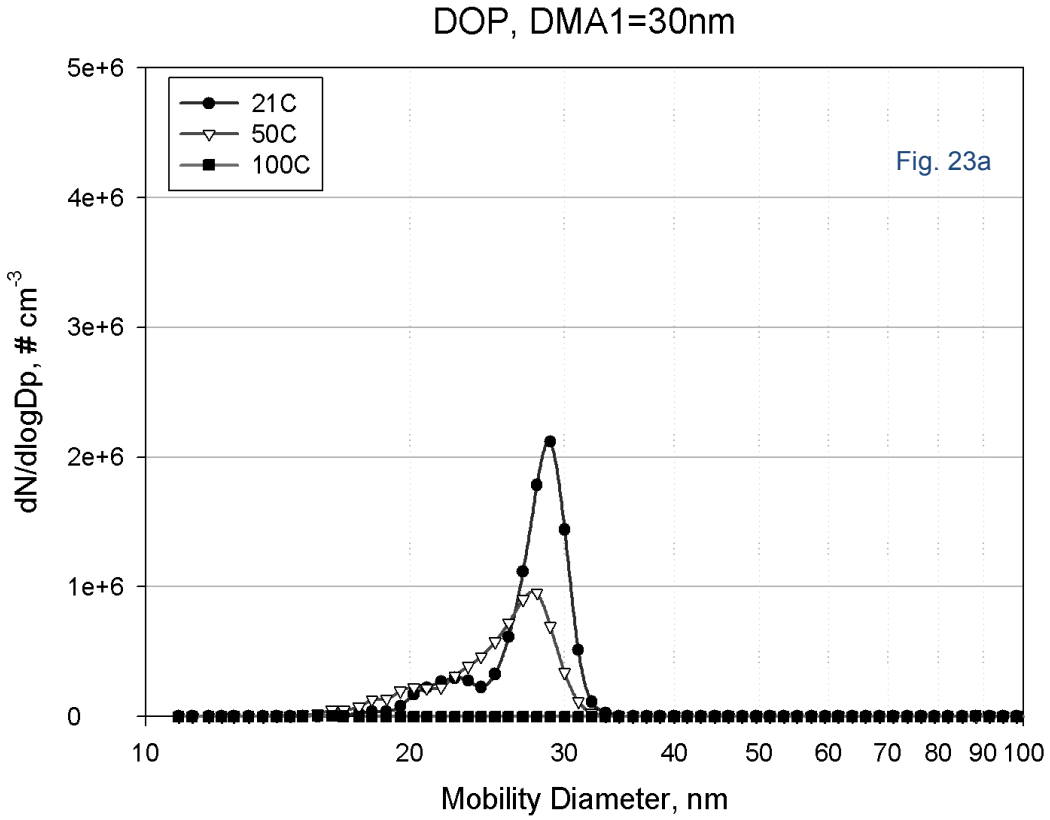

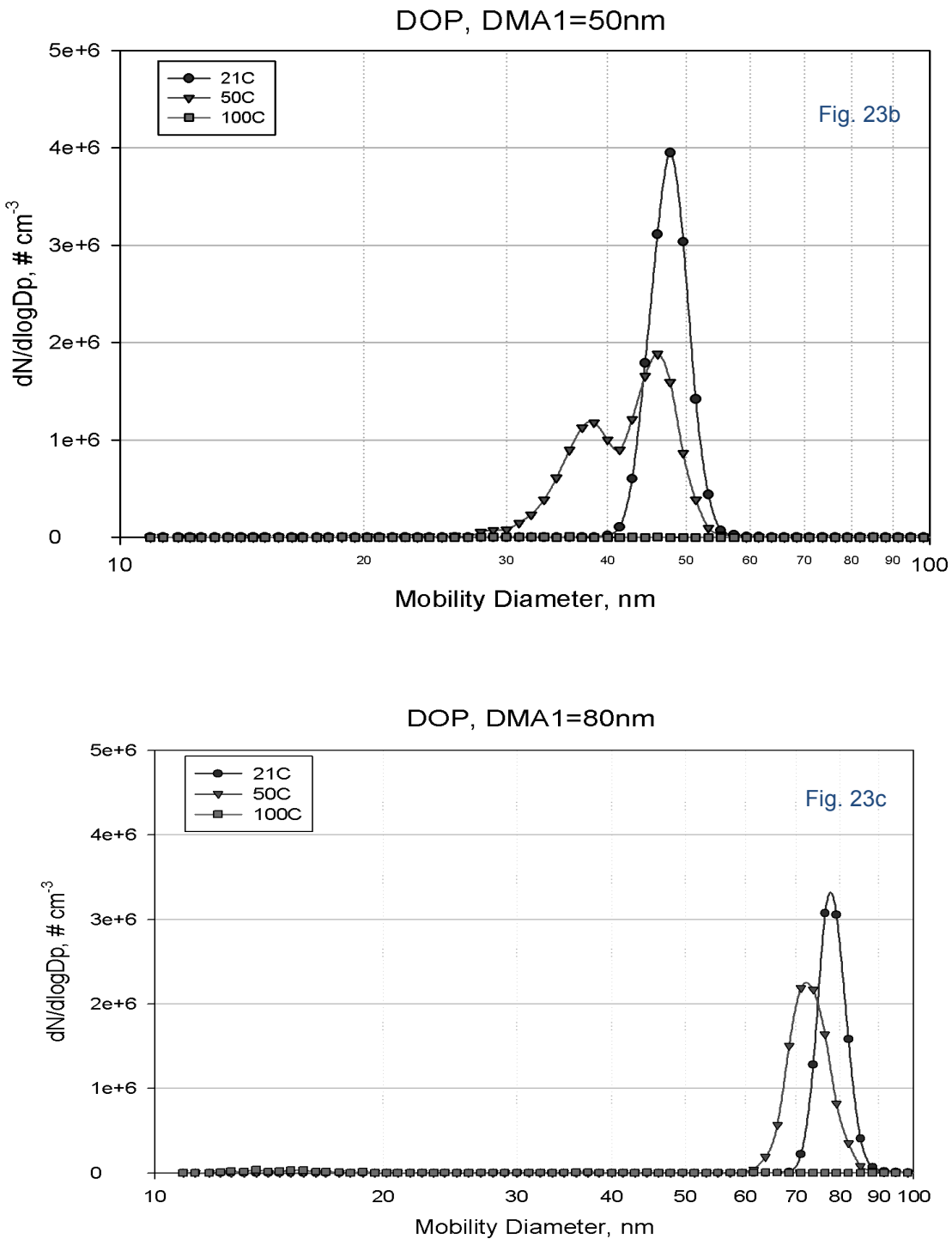

Figure 23. Size distribution of monodisperse DOP particles as a function of temperature

The size distribution of the 30-nm DOP particles appeared to be slightly bimodal with a small hump found at the neighborhood of 20 nm at 21°C. This small hump is likely due to the presence of doubly charge particles of imprecisely selected DOP particles (that are oil droplets), because as a doubly charge 30-nm particle would have twice the electrical migration velocity (equivalent of electrical mobility) as that of a singly charged particle. A doubly charged 30-nm DOP droplet would then be classified as a smaller 15-nm, for example, and registered in the size spectrum in Figure 23a. This assumption implies that some larger oily DOP particles acquire more charges in the charger region before entering the DMA1. If no additional processes occurring in DMA1, this doubly charged DOP particles should have been resolved in a single peak in the size spectrum shown in Figure 23a. Instead, we saw a continuous hump not a single peak suggesting a range of large particles were doubly or triply charged, which is an unlikely scenario for the nice continuous hump section.

An alternative hypothesis is that ethanol is expected to evaporate faster from the 30-nm particles than that from the 50- or 80-nm particles due to the curvature effect even at the room temperature. This could create a small sub-population of particles that forms the hump in Figure 23a, but this would have to imply that the classified 30-nm particles continue to shrink in DMA1 through the evaporation of ethanol from the 30-nm DOP particles, which is a more reasonable assumption than the multiple charging assumption stated above. Furthermore, this small hump should not affect the focus of this study, because at the 21°C the hump was not found in the 50-nm (Figure 23b) or 80-nm curves (Figure 23c) that further supports the hypothesis that the small hump was caused by evaporation of ethanol from the 30-nm particles. Larger particles have smaller vapor pressure and retain molecules better than smaller ones.

As the temperature in the heating section was increased to 50°C from the room temperature of 21°C, the small hump in Figure 23a disappeared and the left wing of the curve was elevated slightly to form a heavier tail for the 30-nm incoming DOP particles. Note that the 30-nm peak height was also reduced by more than 50% indicating a significant loss of 30-nm DOP particles. These results are indicative of thermal effects on the 30-nm DOP particles. A distinct peak of DOP particle about 38nm was found in Figure 23b for the 50-nm incoming DOP particles. Invoking the ethanol evaporation hypothesis could explain well for the formation of the 38-nm peak in the 50-nm incoming DOP particles. Again, the main 50-nm peak was reduced by about 50% in height consistent with that of 30-nm peak. No secondary peak was found in the 80-nm case as shown in Figure 23c as the heating temperature increased from 21 to 50°C. However, the 80-nm peak was also reduced by about 50% as the temperature increased. These results all suggest that as the heating temperature was increased from 21 to 50°C the DOP particles would be halved in number, which suggest the particulate material loss was achieved through the evaporation process. The inconsistency in the formation dynamics of secondary peak was due to the ethanol used in the preparation of DOP stock solution and different evaporation process of ethanol from that of DOP as a function of temperature and particle size.

The left shift of the peak particle size as the heating temperature changed was not as prominent as that of particle number for the DOP particles (see Figure 23a, b, and c). The left shift was less than 2 nm for the 30- and 50-nm incoming particles, and less than 6nm for the 80-nm incoming DOP particles. These were detectable change of particle size, but it was again not as significant as that of the particle number concentration discussed above.

The behavior of nanoparticles in a thermal field as in the VPS is similar for materials other than NaCl discussed in the last Section (III.2.2.1) and DOP in this Section. These include ammonium sulfate, sucrose, nano-silver, and nickel chloride. **In other words, these tested nanoparticles could be evaporated as the VPS heating temperature increased thereby reducing the number concentration. The temperature for complete evaporation (or 100% reduction/removal of the particle number concentration) of the entire particle population is material dependent. The thermal factor only has a minimal effect on the population size of monodisperse particles, not as significant as that on the**

particle number concentration. Finally, the temperature required to vaporize nanoparticles appear to be much less than that required for bulk and much larger grain size materials where the melting point was measured. It is important that the VPS be evaluated for carbonaceous particles other than sucrose, such as engine soot, which we will show in the later Sections.

(III.2.2.3) Rate of Thermal Removal of Nanoparticles

The complete removal of a particle population depends on several factors in operating an instrument like the VPS or any other VPR devices such as a thermodenuder and catalytic stripper. These factors are the residence time of the particles in the device (thus flow rate dependent) and the "vaporization temperature" of the particles (thus material and size dependent). To achieve a high thermal removal of nanoparticles for a given device one needs to understand the kinetics or the rate of removal of the material of that device. This section will present our limited data toward understanding the removal kinetics of nanoparticles in VPS.

The thermal effects on evaporation of nanoscale particles are discussed using the plot of Figure 24. The number fraction of particles remained after the thermal evaporation step is plotted as a function of heating temperature in this figure for two selected nanoparticles – NaCl and DOP. As a general observation, the nanoparticles are thermally removed (i.e., evaporated) as the heating temperature increased. The removal rate as a function of temperature is strongly dependent on the material (e.g., NaCl particles require significantly higher temperature to vaporize than DOP particles do) and the size of the nanoparticles (e.g., 80nm particles requires higher temperature to be completely vaporized than 17nm ones at the same VPS operating condition). The 30-nm DOP particles vaporized faster than the 80-nm particles. For the curves in the DOP group in Figure 24, there is an evidence of slight difference in the removal rate due to the difference in the Qv (flow through the membrane, i.e., 1.5 vs. 0.5 lpm). A higher Qv represents a shorter residence time in the VPS, which is consistent with our finding that the impact of Qv is slightly higher for the smaller DOP particles (30 nm) than for the larger ones (80 nm). Similar observations were also found for NaCl particles.

The residence-time effect on the thermal kinetics of nanoparticle removal is thus universal for nonvolatile and volatile particles. It is important to note that the response of the smallest NaCl nanoparticles to the heating temperature is contrasting to that of the larger ones, but it appears to be consistent with other literature reports on nanoparticles. Given the same material, particles will evaporate faster as their sizes become smaller. The evaporation rate might have a low threshold limit below which the nanoparticles would completely vaporized instantly upon entering the heating section of the VPS.

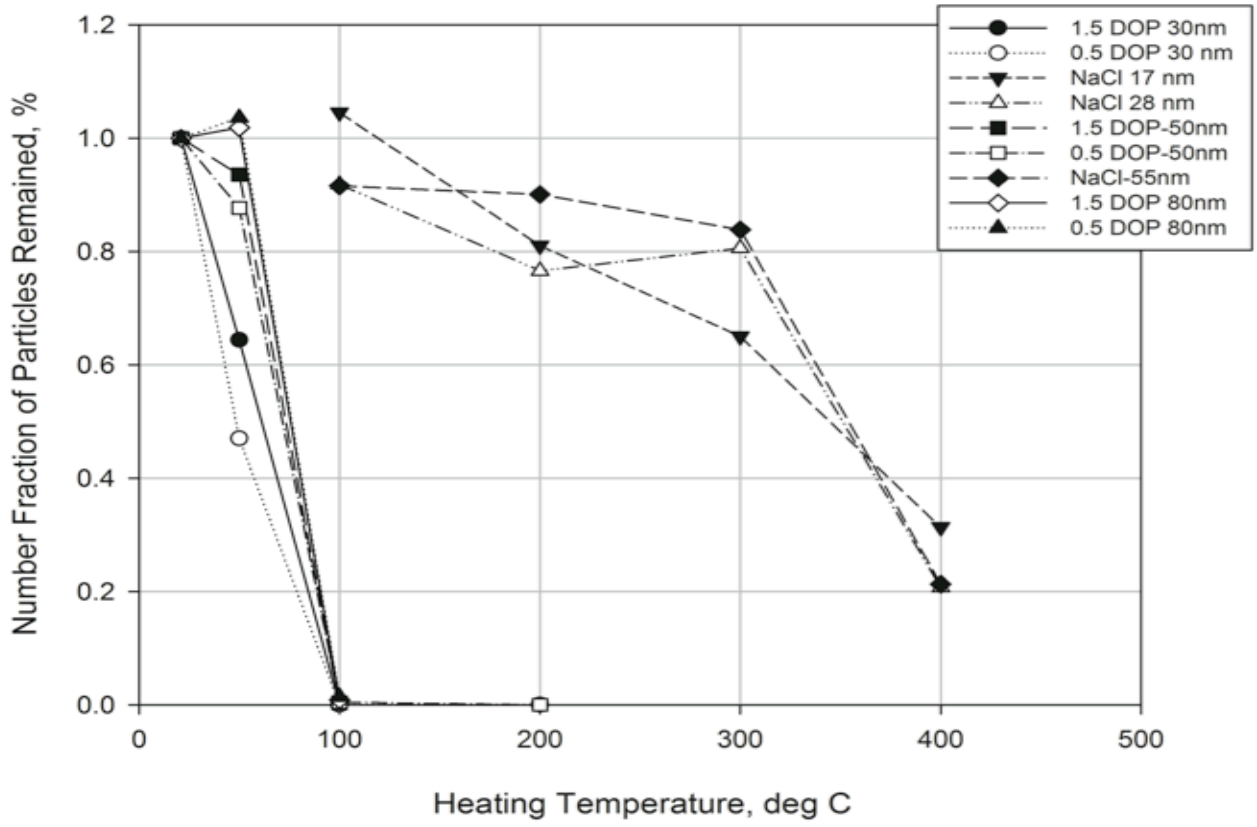

Figure 24. Evaporation kinetics of various nanoparticles

(III.2.2.4) VPS Applications in Engine Particles

To further evaluate the VPS, we had performed limited tests on engine-emitted particles. One of these tests is using particles emitted by a diesel engine operated under **c**onventional **d**iesel **c**ompression (CDC) mode at the National Transportation Research Center (NTRC) in Oak Ridge National Laboratory. Figure 25 illustrates the TDMA setup for the CDC experiment. Figures 26 and 27 show the photos taken during the CDC experiments at NTRC.

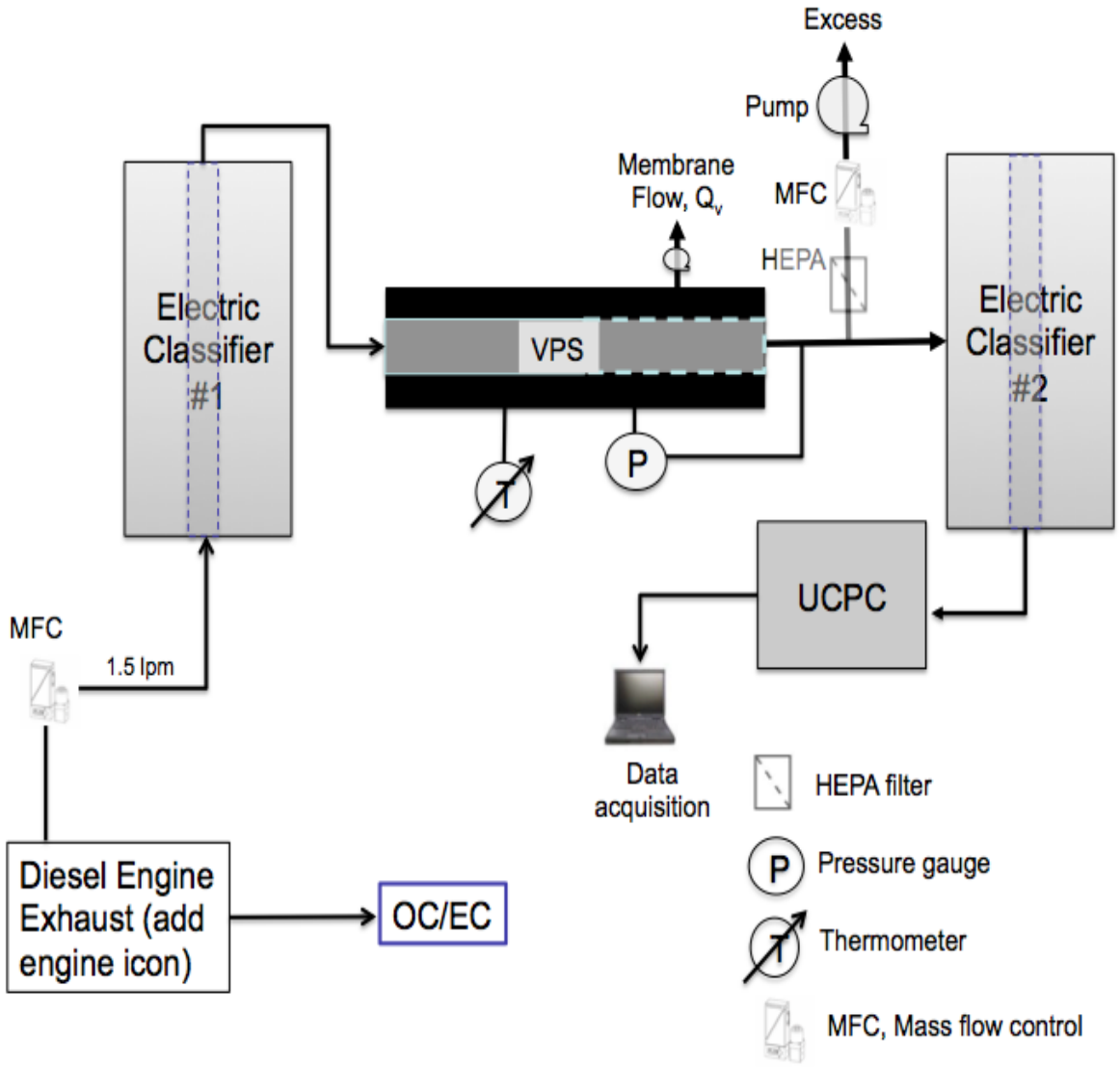

Figure 25. TDMA setup for diesel engine experiment at NTRC

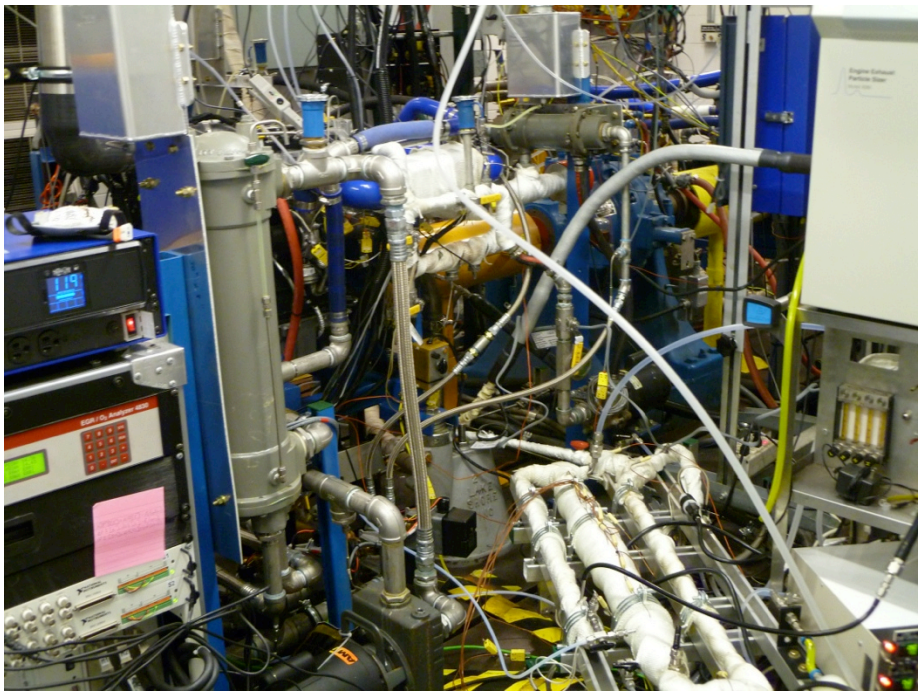

Figure 26. Photo of the diesel engine apparatus at NTRC

Shown in the center on the floor is the PMP (in white thermal blanket wrapping in the lower right hand side), the photoacoustics sensor is toward the left side of the photo, while the flow control and array of sensors are toward the right hand side of the photo.

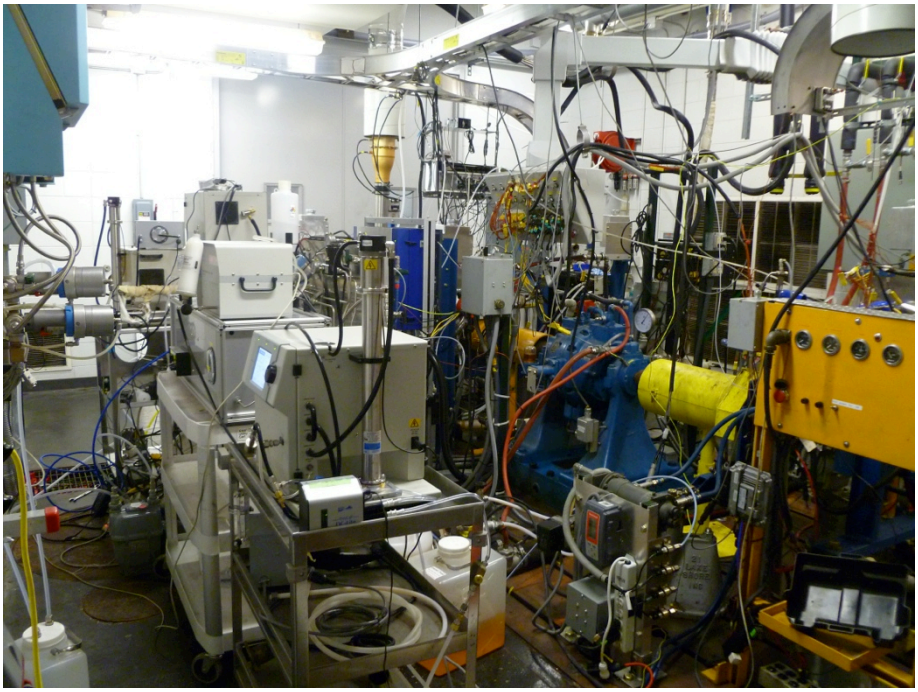

Figure 27. Photo of the TDMA-VPS setup at NTRC

(III.2.2.5) Thermal evolution of diesel engine particles under CDC operating mode

The performance of the VPS was tested further using real engine particles emitted by the diesel engine operated at the CDC mode. The thermal behavior of the exhaust particles from the conventional diesel engine combustion was investigated also using TDMA technique to provide monodisperse engine particles extracted by DMA1 (see Figure 25). Three DMA1-selected sizes of particles were 95, 52 and 18nm from the broadband CDC engine particle size distribution that was peaked at around 52nm. The geometric standard deviations of the selected particle sizes (as shown in the 25C curve of Figures 28a, b, and c) were all less than 1.2 indicating monodisperse population at the three sizes for VPS test. The VPS was operated at the five pre-set temperatures (25, 100, 200, 300, and 350°C).

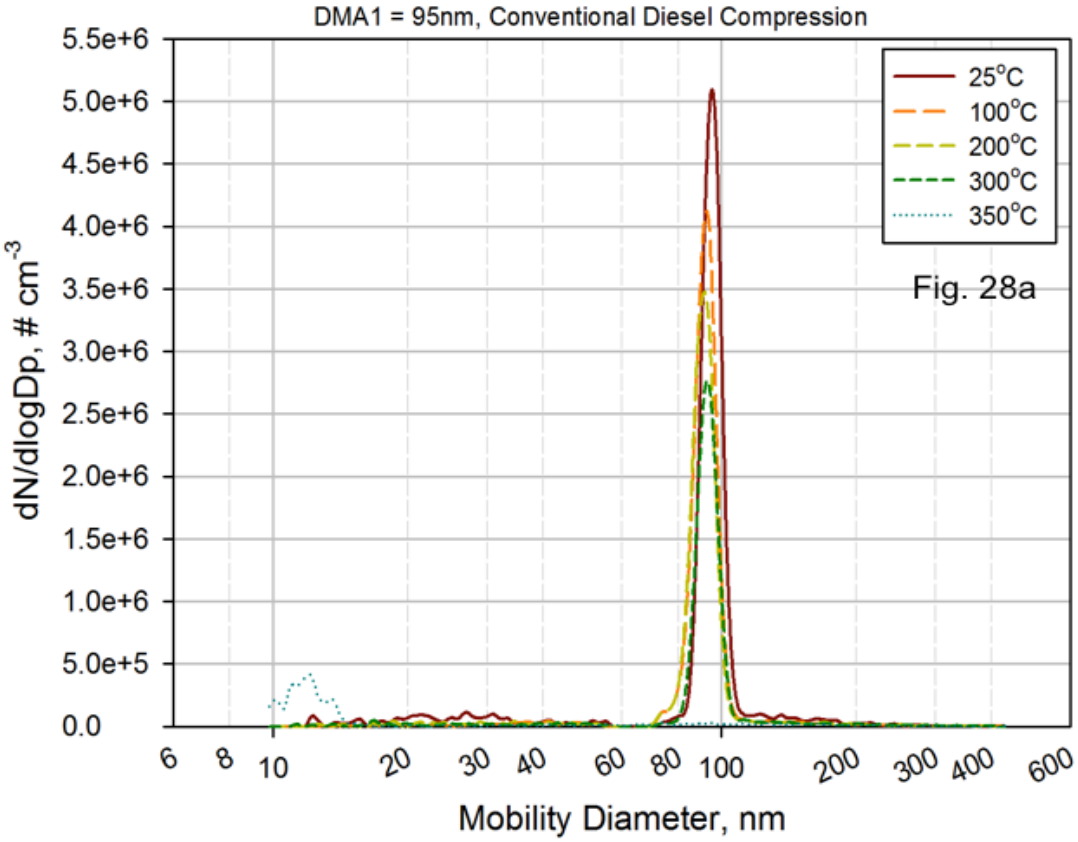

The peak size of the incoming 95-nm particles changed slightly from 25 to 300°C, although the peak height decreased from approximately $5x10^6$ at 25°C to $2.7x10^6$ at 300°C. As shown in Table 1, the number of the incoming 95-nm particles decreased as the temperature increased until it reached 350°C. At 350°C, loss of particles occurred at a much greater extent than that at any lower temperatures and the remnant of the 95-nm particle population was barely detectable.

The VPS data on nonvolatile particles such as NaCl (Figure 22) indicate that the peak number concentration would decrease as the heating temperature increases, but the peak size or location would not change much. The observation of the relatively constant peak size at 95nm (± 2nm) in Figure 28a as the temperature increased appears to be consistent with our previous observations using the pure

compound. Does this imply that 95-nm CDC particles are mostly nonvolatile particles?

As the incoming CDC particles were downsized from 95-nm to 52nm, we found the thermal behavior is slightly different from that displayed in Figure 28a and the 52-nm results are shown in Figure 28b. The peak height also decreased accordingly to the increase of temperature for the 52-nm incoming particles. However, we saw that the peak location (the peak size) started to shift to the left of the 52-nm peak. The reduction in the incoming peak size as the temperature increase is consistent with those of volatile particles like the DOP particles (Figure 23). Again, all 52-nm CDC particles disappeared at 350°C.

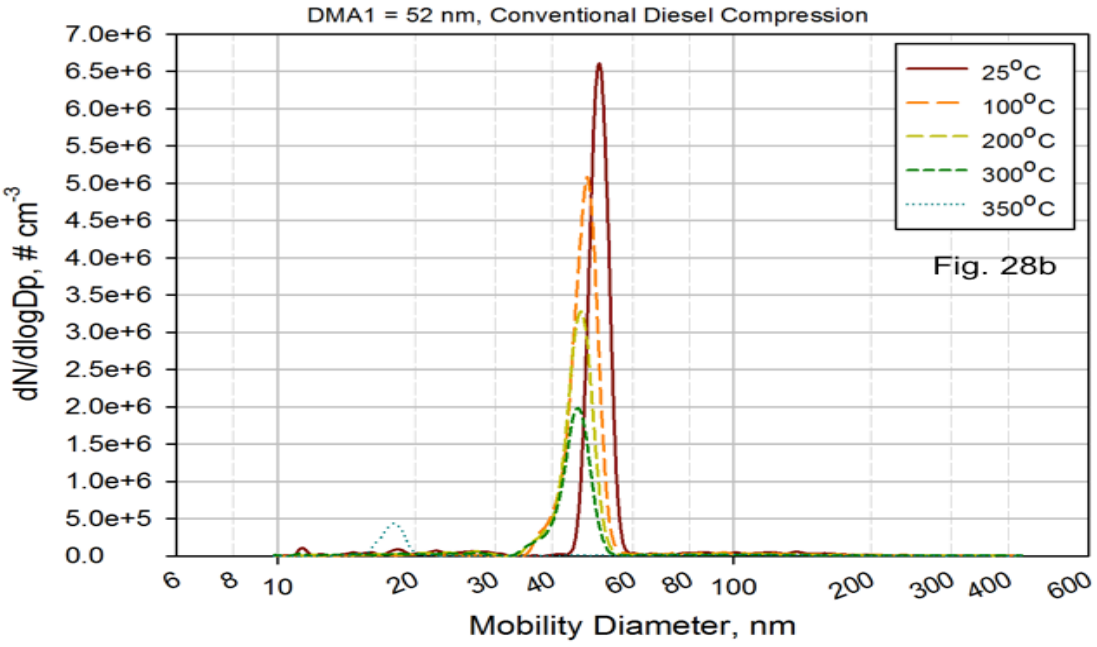

The thermal behavior of the incoming 18-nm CDC particles as function of temperature is shown in Figure 28c. We noticed that the change in the peak particle size is substantially larger than that in the previous two larger sizes. Furthermore, it does not take 350°C to vaporize entire 18-nm particle population. The peak height was at $1.7x10^6$ at 25°C and that was at $5x10^5$ at 200°C in Figure 28c. That is about 71% loss. By the time the temperature reached 300°C, the SMPS was unable to detect any particles. Even the size distributions at 100 and 200°C was not a single-mode like that at 25°C. In other words, the particle population became polydisperse from the original monodisperse distribution simply due to the increase of temperature. That is a clear indication that the 18-nm particles are most likely to be volatile in nature.

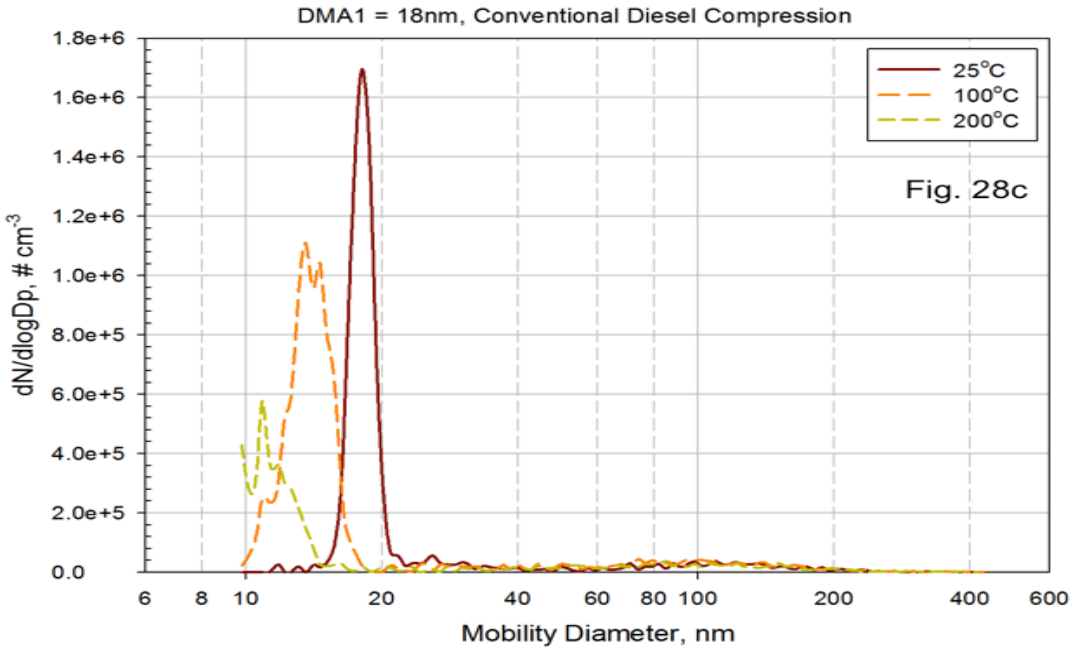

Figure 28. Size distribution of monodisperse CDC engine particles in response to temperature variation in VPS (a=95nm, b=52nm, c=18nm)

Finally, the behavior of the CDC diesel engine particles with respect to the applied thermal energy (or heating temperature), defined by the number concentration, is consistent with those we learned for the laboratory-generated particles and reported in literature (e.g., Ristimaki et al., 2007). In other words, particle number concentration would significantly decrease as the heating temperature increased to a critical point. The rate of particle loss (as in the reduction of number concentration) appears to be higher for smaller particles (e.g., 18-nm) than for the larger ones (52-nm and 95-nm) given the same material.

Table 1. Statistical Summary for Particle Number Concentration in CDC Data

	Fraction Evaporated (%)		
T (°C)	18nm	52nm	95nm
25	0%	0%	0%
100	35%	18%	19%
200	67%	29%	40%
300	99%	44%	45%
350		93%	92%

Change of the particle size statistics in response to heat are shown in Table 1. The VPS was performed as expected that the particles were removed as the temperature increased, and at 350°C greater than 92% of the particles were removed. Although PMP requires 99% of total particle removal, we think the result suggests that the VPS is a promising technology.

The shift of the 95-nm peak (defined as the mode diameter) is very little from 25 to 300°C and has no defined direction. We assume that the 95nm incoming particles were mostly soot, which would require a temperature higher than 350°C to vaporize effectively. The data appear to support this hypothesis.

With the 52-nm incoming CDC particles, the progressively left-shift of the peak size as the temperature increased was observed (see Table 2). Similar observation was found for the 18-nm incoming CDC engine particles (see Table 2). This is also consistent with our previous findings using laboratory-generated particles. The data at 350°C shown in Table 2 further suggests that the thermal behavior of the CDC engine particles of all 3 incoming sizes are consistent with the data obtained from laboratory-generated particles in that they will change a little but not significantly, until they reach a critical temperature where many of them were vaporized. At that instance, the population will be changed and the statistics (peak size and broadening) associated with this change support this conclusion.

Table 2. Statistical Summary of Particle Diameter in CDC Data

	Mode Diameter Shift (nm)		
T (deg C)	18nm	52nm	95nm
25	0.0	0.0	0.0
100	-4.5	-3.6	-3.3
200	-7.2	-5.3	-3.3
300		-5.3	0.0
350		nc	nc

nc: not computed due to non-distribution

It is likely that larger particles were composed of soot and higher molecular weight species that requires more thermal energy to vaporize than that in small particles that consist of mostly lower molecular weight or volatile species. Larger soot particles have more complex morphology (e.g., fractal structure) that could shield condensible molecules or attract the molecules strongly, while small particles do not have such ability to shield condensibles. Most of the condensibles would be exposed to the surface of small soot particles. Even the smaller size particles could be composed of entirely condensibles. Thus, the distributions of the 95- and 52-nm particles changed little as the temperature increased until it reached about 350°C when the particle populations vaporized almost completely. On the other hand, the 18-nm particles could consist of lower molecular weight species that were completely vaporized even at 200°C.

(III.3) Tests of DC-VPS Integrated System Using T63 Engine-Generated Particles

Coupling of the DC and VPS as an integrated system for volatile engine particle measurement was tested using the T63 engine available at the Wright-Patterson Air Force Research Laboratory. The setup was illustrated in Figure 6. The stable size distributions taken at three temperature settings during a T63 engine experiment in April 2010 are displayed in Figure 29. The engine was operated at idle condition and the dilution ratio is 10:1 for the data displayed in Figure 29; the number concentration was dilution-corrected. It is known from the experience operating the T63 engine at the Wright-Patterson AFRL that the volatile fraction is the highest in the emissions compared with that operated at cruise and max engine power conditions.

The peak location of any of the three particle size distributions shifts to the left (size reduced) as the heating temperature increased (see Figure 29). This observation is consistent with those observed in the CDC diesel engine emissions and the synthetic volatile particles. The size reduction was most

pronounced from the unheated condition to 200°C, about 7 nm, as compared to that of 2.6 nm from 200 to 300°C. The peak height (i.e., the particle number concentration) is reduced as the temperature increased.

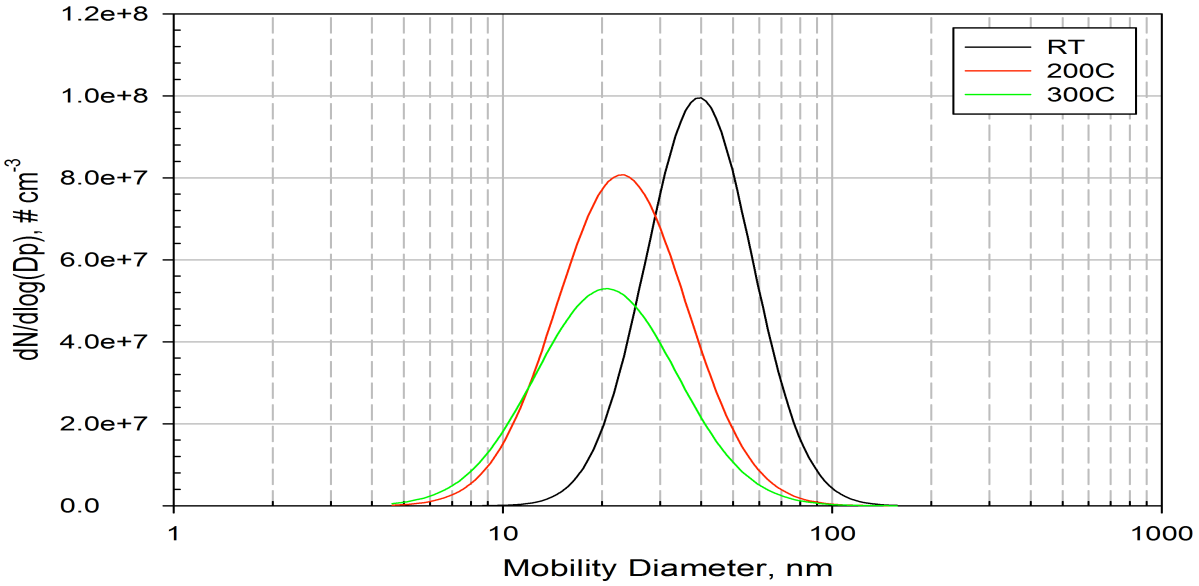

Figure 29. Size distributions of particles taken during an idle T63 engine operation

The size distributions as the temperature change for the same T63 engine operated at a higher power condition, the cruise condition, is shown in Figure 30. The shift of size distribution as a function of temperature shown in Figure 30 for the cruise power condition is in the opposite direction from that in Figure 30 in the idle condition. The increase in the peak height is 10 nm from the unheated to 200°C and less than 1 nm from 200 to 300°C.

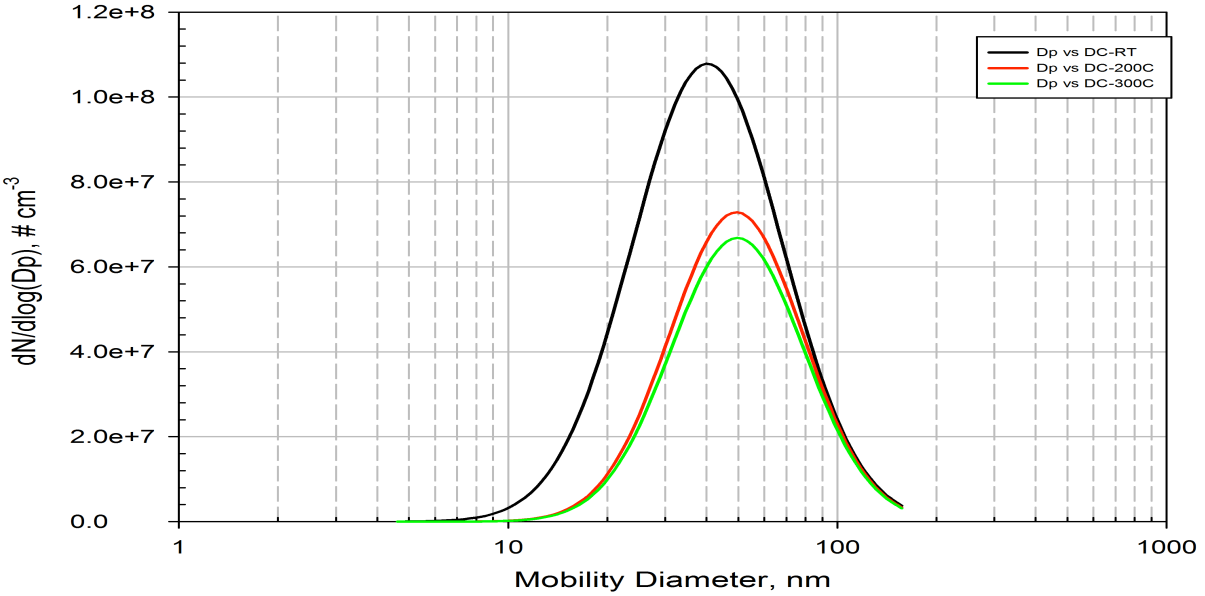

Figure 30. Size distributions of cruise T63 engine emissions

Note that the keyword here is “increase” in the peak size as the temperature increased for the cruise condition. If the particles were volatile, we would expect the peak to shift to a smaller size not to a

larger size as we had seen in the CDC and DOP particles. Why there is such a discrepancy? Based on what we have learned in this project we think the following scenario is likely: For the cruise condition, the volatile particles in the total particle population evaporated as the temperature increased. Since these volatile particles were "likely" to be in the smaller size range, their loss could change the particle population statistics and led to the right shift of the distribution shown in Figure 30. If this is true, that means volatile particles are mostly in the smaller size region of the curve, which is also consistent with higher number concentration.

As the heating temperature goes from 200°C to 300, most of the volatiles were removed from the particle population leaving those nonvolatile soot particles. Thus, the peaks of the red and green curves are in the same location as seen in Figure 29. The T63-cruise power engine emitted particles larger than approximately 70 nm are simply insensitive to temperature increase. The difference in the size location of these two last curves is minimal in this case. For the idle condition in Figure 29, however, the particles are mostly wet meaning they are volatiles or evaporable, could be entirely in a droplet state (similar to that of DOP discussed earlier, for example). Thus, its thermal behavior shown in Figure 29 appears to be similar to those shown in Figure 23.

(IV) CONCLUSIONS

Volatile particles are a major component of atmospheric aerosols, and by-products of atmospheric transformation from precursors generated by aircraft engines and many other sources of anthropogenic and natural origins. Volatile particles do not present themselves as "particles" as in a condensed or particulate state, but they will emerge and be detectable as particles when they are downstream of an aircraft engine exhaust nozzle. The knowledge about aircraft, especially military aircraft's, contribution to the formation of volatile components in the atmospheric aerosol is inadequate and currently subject to great uncertainty. One of the major uncertainties is related to the quality of volatile particle data that currently exist.

Volatile particles are extremely challenging to sample and measure at the present. These particles and their precursor species are highly transitional in nature, which render its quantitative determination highly difficult if not impossible. The partition of the volatile components depends on the properties of the condensing molecules and quantity of the active particle surface, which is a function of temperature and pressure. Through this project we have developed prototype devices, tested these devices in laboratory and field conditions using synthetic and engine emitted particles. Most importantly we have been able to learn the fundamental behavior of nanoparticles that are consisted of pure and mixed material properties in dry and wet states. The knowledge helps interpreting the data produced by the new instruments (DC and VPS) developed in this project.

We have learned that:

- DC has the capability to preserve the size distribution of engine particles and appears to possess no drawbacks that a tip-diluting probe has in sampling aircraft engine particles. The promising result opens the door for DC to replace the tip-diluting probe.
- VPS has a high particle transmission efficiency and ability to scan temperature to generate a thermograph that is critical to understand engine aerosol volatility. The transmission efficiency is independent of material composition of the particles. This capability qualifies VPS an instrument uniquely suited for measurement of volatile engine particles.
- Population of particles in droplet state and or containing mostly volatile species will left-shift in size distribution when they encounter a thermal field. Their number concentration will also be reduced through evaporation leading to active particle-to-gas mass transfer.

- Population of particles in a mixed state (consisting of solid soot and condensibles) will right-shift when they encounter a thermal field. Their number concentration will also be reduced through evaporation of volatile particles.
- Nanoparticles appear to have a lower mass transfer barrier (a smaller exponent in the Arrhenius equation) than their larger counter part. For example, bulk salt has a boiling point and melting point way higher than 800°C. The nanoparticles made of the same salt could be completely vaporized in VPS in 400.
- A new system configured of DC-VPS could provide a viable solution to address the needs in volatile engine particle sampling and measurement.

In summary, we conclude that we have accomplished all the goals proposed for this SERDP WP-1627 project. The prototype devices delivered useful data for advancing the science of engine emissions measurement and aerosol volatility. The results will become the foundation for any future work in sampling and measurement of volatile engine particles.

(V) POTENTIAL FUTURE APPLICATIONS

The two prototype devices (DC and VPS) are generic and can be applied in many areas ranging from engine emissions, combustion diagnostics, fuel development, fuel and engine certification, secondary aerosol formation, and nanotechnology.

Ongoing research projects are utilizing VPS to obtain the volatile components and mixing state of aerosol in material science that is funded by DOE Energy Efficiency and Renewal Energy Research (EERE) and Vehicle Technology Research Program at NTRC, while another project is using VPS to assist obtaining the aerosol thermogram for characterizing charge carriers funded by Defense Advanced Research Projects Agency (DARPA).

Both DC and VPS will require further demonstration and field tests before commercial implementation is possible.

(VI) REFERENCES

Aerospace Information Report 5892 (2012) *Nonvolatile exhaust particle measurement techniques*, SAE publication (STABILIZED Mar 2012).

An, W. J., Pathak, R. K., Lee, B.-H., Pandis, S. N. (2007) Aerosol volatility measurement using an improved thermodenuder: Application to secondary organic aerosol. *J. Aerosol Sci*., 38, 305-314.

Andersson, J., Clarke, D. (2004) *UN-GRPE PMP phase 3: inter-laboratory correlation exercise: framework and laboratory guide*, http://www.unece.org/trans/doc/2005/wp29grpe/PMP-2005-14-01e.pdf.

Bird, R. B., Stewart, W. E., Lightfoot, E. N. *Transport Phenomena*, Wiley, New York, 1960.

Bulzan, D., Anderson, B., Wey, C., Howard, R. (2010) Gaseous and Particulate Emissions Results of the NASA Alternative Aviation Fuel Experiment (AAFEX). *Proceedings of the ASME Turbo Expo*, Glasgow, Scotland, June 14-18. GT2010-23524.

Busen, R., Schumann, U. (1995) Visible contrail formation from fuels with different sulfur content. *Geophys. Res. Lett.,* 22**,** 1357.

Burtscher, H., Baltensperger, U., Bukowiecki, N., Cohn, P., Huglin C., Mohr, M., Matter, U., Nyeki, S., Schmatloch, V., Streit, N., Weingartner, E. (2001) Separation of volatile and nonvolatile aerosol fractions by thermodesorption: instrumental development and applications. *J. Aerosol Sci*., 32, 427-442.

Burtscher, H. (2005) Physical characterization of particulate emissions from diesel engines: a review. *J. Aerosol Sci.,* 36, 896-932.

Chen, D.-R., Pui, D.Y.H., Hummes, D., Fissan, H., Quant, F. R., Sem, G. J. (1998) Design and evaluation of a nanometer aerosol differential mobility analyzer (Nano-DMA). *J. Aerosol Sci*., 29, 497-509.

Chen, D.-R., David Y.H. Pui, Stanley L. Kaufman (1995) Electrospraying of conducting liquids for monodisperse aerosol generation in the 4 nm to 1.8 μm diameter range, *J. Aerosol Sci*., 26, 963-977.

Cheng, M.-D. and Steve E. Allman (2011) Improved measurement of volatile particles: Vapor-particle separator design and laboratory tests, *Rev. Sci. Instr*., 82, 125106, 8 pages.

Cheng, M.-D. (2004) Effects of Nanophase Materials (<= 20 nm) on Biological Responses, *J. Environ. Sci. & Health*, invited, A39, 2,691-2,705.

Cheng, M.-D., Corporan, E., DeWitt, M. J., Spicer, C. W., Holdren, M. W., Cowen, K. A., Laskin, A., Harris, D. B., Shores, R. C., Kagann, R., Hashmonay, R. (2008) Probing emissions of military cargo aircraft: description of a joint field measurement Strategic Environmental Research and Development Program. *J. Air Waste Manage.,* 58, 787-796.

Cheng, M.-D., Corporan, E., DeWitt, M. J., Landgraf, B. (2009) Emissions of volatile particulate components from turboshaft engines operated with JP-8 and Fischer-Tropsch fuels. *J. Aerosol Air Quality Res.,* 9, 237-256.

Cheng, M.-D. (2010) Development and application of a membrane-based thermodenuder for measurement of volatile particles emitted by a jet turbine engine. *Proceeding of ASME Gas Turbine Congress*, June 14-18. GT2010-22175.

Cobourn, W. G., Husar, R. B., Husar, J. D. (1978) Continuous in-situ monitoring of ambient particulate sulfur using flame photometry and thermal analysis, *Atmos. Environ*., 12, 89-98.

Corporan, E., Quick, A., DeWitt, M. J. (2008) Characterization of particulate matter and gaseous emissions of a C-130H aircraft, *J. Air Waste Manage*., 58, 474-483.

Corporan, E., DeWitt, M. J., Klingshirn, C. D., Anneken, D. (2011) Alternative Fuels Tests on a C-17 Aircraft: Emissions Characteristics, USAF AFRL Technical Report, AFRL-RZ-WP-TR-2011-2004.

Crayford, A., Johnson, M., R. Marsh, R., Sevcenco, Y., Walters, D., Williams, P., Christie, S., Chung, W., Petzold, A., Ibrahim, A., Delhaye, D., Quincey, P., Bowen, P., Coe, H., Raper, D., Wilson, C. (2011) SAMPLE III: Contribution to aircraft engine PM certification requirement and standard First Specific Contract, Final Report, 21st October 2011, EASA.2010.FC.10.

CRC *Handbook of Chemistry and Physics* (2009), the 90th Edition, Lide, D.R. ed., Boca Raton, FL.

Donahue, N.M., Robinson, A. L., Stanier, C. O., Pandis, S. N. (2006) Coupled partitioning, dilution, and chemical aging of semivolatile organics. *Environ. Sci. Technol.,* 40, 2635-2643.

Fierz, M., Vernooij, M. G. C., Burtscher, H. (2007) An improved low flow thermodenuder, *J. Aerosol Sci.,* 38, 1163-1168.

Fuchs, N. A., Sutugin, A. G. (1971) A model for particle formation and growth in the atmosphere with molecular resolution in size, In G. M. Hidy and J. R. Brock (Eds.), Topics in current aerosol research (Part 2) (pp. 1791-1807). Pergamon, New York.

Giechaskiel, B., Chirico, R., DeCarlo, P. F., Clairotte, M., Adam, T., Martini, G., Heringa, M. F., Richter, R., Prevot, A. S. H., Baltensperger, U., Astorga, C. (2010) Evaluation of the particle measurement programme (PMP) protocol to remove the vehicles' exhaust aerosol volatile phase. *Sci. Total Environ.,* 408, 5106-5116.

Howard, R. P., Hiers, R. S., Whitefield, P. D., Hagen, D. E., Wormhoudt, J. C., Miake-Lye, R. C., Strange, R. (1996) Experimental characterization of gas turbine emissions at simulated flight altitude conditions, AEDC-TR-96-3, Final Report.

Huffman, J. A., Ziemann, P. J., Jayne, J. T., Worsnop, D. R., Jimenez, J. L. (2008) Development and Characterization of a Fast-Stepping/Scanning Thermodenuder for Chemically-Resolved Aerosol Volatility Measurements. *Aerosol Sci. Technol*., 42, 395-407.

Johnson, G. R., Ristovski, Z., Morawska, L. (2004) Method for measuring the hygroscopic behavior of lower volatility fractions in an internally mixed aerosol. *J. Aerosol Sci.,* 35,443-455.

Liu, B. Y. H., Pui, D. Y. H., Whitby, K. T., Kittelson, D. B. (1978) The aerosol mobility chromatograph: a new detector for sulfuric acid aerosols, *Atmos. Environ*. 12, 99-104.

Maricq, M. M., Xu, N. (2004) The effective density and fractal dimension of soot particles from premixed flames and motor vehicle exhaust. *J. Aerosol Sci.,* 35, 1251-1274.

Maricq, M. M. (2007) Chemical characterization of particulate emissions from diesel engines: a review. *J. Aerosol Sci.,* 38, 1079-1118.

Newman, L. (1978) Techniques for determining the chemical composition of aerosol sulfur compounds. *Atmos. Environ*., 12,113-125.

NIST, http://webbook.nist.gov/cgi/cbook.cgi?ID=C7647145&Mask=4&Type=ANTOINE&Plot=on

Pankow, J. F. (1994) An absorption model of gas aerosol partitioning involved in the formation of secondary organic aerosol. *Atmos. Environ*., 28, 185-188.

K. Park, D. Dutcher, M. Emery, J. Pagels, H. Sakurai, J. Scheckman, S. Qian, M.R. Stolzenburg, X. Wang, J. Yang, and P.H. McMurry (2008) Tandem Measurements of Aerosol Properties—A Review of Mobility Techniques with Extensions, *Aerosol Sci. Technol.*, 42:801-816.

Park, D., Kim, S., Choi, N. K., Hwang, J. (2008) Development and performance test of a thermodenuder for separation of volatile matter from submicron aerosol particles. *J. Aerosol Sci*., 39, 1099-1108.

Phelps, T. J., Palumbo, A. V., Bischoff, B. L., Miller, C. J., Fagan, L. A., McNeilly, M. S., Judkins, R. R. (2008) Micron-pore-sized metallic filter tube membranes for filtration of particulates and water purification. *J. Microbial Methods.,*74, 10-6.

Rader, D. J., McMurry, P. H. (1986) Application of the tandem differential mobility analyzer to studies of droplet growth or evaporation. *J. Aerosol Sci*., 17, 771-788.

Riipinen, I., Pierce, J. R., Donahue, N. M. Pandis, S. N. (2010) Equilibration time scales of organic aerosol inside thermodenuders: Evaporation kinetics versus thermodynamics. *Atmos. Environ*., 44, 597-607.

Ristimaki, J., Vaaraslahti, K., Lappi, M., Keskinen, J. (2007) Hydrocarbon condensation in heavy- duty diesel exhaust. *Environ. Sci. Technol*., 41, 6397- 6402.

Robinson, A. L., Donahue, N. M., Shrivastava, M. K., Weitkamp, E. A., Sage, A. M., Grieshop, A. P., Lane, T. E., Pierce, J. R., Pandis, S. N. (2007) Rethinking Organic Aerosols: Semivolatile Emissions and Photochemical Aging, *Science*, 315, 1259-1262.

Robinson, A. (2011) Measurement and modeling of volatile particle emissions from military aircraft, Final Report, SERDP Project WP-1626, Oct.

Ronkko, T., Virtanen, A., Kannosto, J., Keskinen, J., Lappi, M., Pirjola, L. (2007) Nucleation mode particles with a nonvolatile core in the exhaust of a heavy duty diesel vehicle. *Environ. Sci. Technol*., 41, 6384-6389.

Rudyak, V.Y., S.N. Dubtsov, and A.M. Baklanov (2009) Measurement of the temperature dependent diffusion coefficient of nanoparticles in the range of 295 to 600K at atmospheric pressure, *J. Aerosol Sci*., 40: 833-843.

Salo, K. (2011) *Physical properties and processes of secondary organic aerosols and its constituents*, Ph.D. thesis, University of Gothenburg, Göteborg, Sweden.

Schumann, U., Arnold, F., Busen, R., Curtius, J., Kärcher, B., Kiendler, A., Petzold, A., Schlager, H., Schröder, F., Wohlfrom, K.-H. (2002) Influence of fuel sulfur on the composition of aircraft exhaust plumes: The experiments SULFUR 1–7. *J. Geophys. Res.,* 107: 4247-4274.

Seinfeld, J. H., Pandis, S. N. (2006) *Atmospheric Chemistry and Physics – From Air Pollution to Climate Change (2nd Ed.)*, John Wiley & Sons, New York, NY.

Slanina, J., Keuken, M. P., Schoonebeek, C. A. M. (1987) Determination of sulfur dioxide in ambient air by means of a computer-controlled thermodenuder system. *Anal. Chem*., 59, 2764-2766.

Sorensen, C. M., Cai, J., Lu, N. (1992) Light-scattering measurements of monomer size, monomers per aggregate, and fractal dimension for soot aggregates in flames. *Appl. Optics,* 31, 6457-6557.

Sturges, W. T., Harrison, R. M. (1988) Thermal speciation of atmospheric nitrate and chloride: a critical evaluation**.** *Environ. Sci. Technol*., 22, 1305-1309.

Swanson, J., Kittelson, D. B. (2010) Evaluation of thermal denuder and catalytic stripper methods for solid particle measurements**.** *J. Aerosol Sci.,* 41, 1113-1122.

Vaden, T. D., Imre, D., Beránek, J., Shrivastava, M., Zelenyuk, A. (2011) Evaporation kinetics and phase of laboratory and ambient secondary organic aerosol*, Proceedings National Academy Sciences,* 108: 2190-2195.

Villani, P., Picard, D., Marchand, N., Laj, P. (2007) Design and Validation of a 6-Volatility Tandem Differential Mobility Analyzer (VTDMA). *Aerosol Sci. Technol*., 41, 898-906.

Wehner, B., Philippin, S., Wiedensohler, A. (2002) Design and calibration of an improved thermodenuder to study the volatility fraction of aerosol particles. *J. Aerosol Sci*., 33, 1087-1093.

Wey, C. C., Anderson, B. E., Wey, C. Miake-Lye, R. C., Whitefield, P., Howard, R. (2007) Overview on the Aircraft Particle Emissions Experiment**.** *J. Propul. Power,* 23: 898-905.

Wu, Z., Poulain, L., Wehner, B., Wiedensohler, A., Herrmann, H. (2009) Characterization of the volatile fraction of laboratory-generated aerosol particles by thermodenuder-aerosol mass spectrometer coupling experiments**.** *J. Aerosol Sci*., 40, 603- 612.

Zheng, M., Cass, G. R., Schauer, J. J., Edgerton, E. S. (2002) Source Apportionment of PM2.5 in the Southeastern United States Using Solvent-Extractable Organic Compounds as Tracers. *Environ. Sci. Technol.,* 36, 2361-2371.

THIS PAGE IS INTENTIONALLY LEFT BLANK.

APPENDIX A - LIST OF PUBLICATIONS

(A.1) Journal Publication and Technical Reports

1. Corporan, E., DeWitt, M.J., Klingshirn, C.D., Anneken, D., "Alternative Fuels Tests on a C-17 Aircraft: Emissions Characteristics," USAF AFRL Technical Report, AFRL-RZ-WP-TR-2011-2004, 2011.
2. Cheng, M.-D. and S. L. Allman (2011) Improved Measurement for Volatile Particles: VPS Design and Laboratory Tests, *Rev. Sci. Instr*. 82(Dec):125106.1-125106.8, doi: 10.1063/1.3665095
3. Cheng, M.-D. (2010) Development and Application of A Membrane-Based Thermodenuder for Measurement of Volatile Particles Emitted by A Jet Turbine Engine, ASME GT2010-22175.
4. Cheng, M.-D. and E. Corporan (2010) A Study of Extractive and Remote-Sensing Sampling and Measurement of Emissions from Military Aircraft Engines, *Atmos. Environ*., 44(2010):4867-4878, doi: 10.1016/j.atmosenv.2010.08.033
5. Corporan, E., M. J. DeWitt, C. D. Klingshirn, R. Striebich, and M.-D. Cheng (2010) Emissions Characteristics of Military Helicopter Engines with JP-8 and Fischer-Tropsch Fuels, *J. Propulsion Power*, 26(2): 317-324, March-April.
6. Cheng, Meng-Dawn, Edwin Corporan, Matthew J. DeWitt, and Bradley Landgraf (2009) Emissions of Volatile Particulate Components from Turboshaft Engines Operated with JP-8 and Fischer-Tropsch Fuels, *J. Aerosol Air Quality Res.*, 9(2): 237-256.

(A.2) Patent Application and Intellectual Properties

1. VPS patent application, MEMBRANE BASED APPARATUS FOR MEASUREMENT OF VOLATILE PARTICLES, US Patent Application, ID 2588, June 2012.

(A.3) Professional Presentations

1. Cheng, M.-D., S. Allman, E. Corporan, M.J. DeWitt, C. Klingshirn, R. Steinbach, T. Barone, and J.M.E. Storey (2011) Effective Separation is the Key to Accurate Measurement of Aircraft Volatile Particulate Matter (WP 1627), The Annual SERDP Symposium, Washington, DC, November.
2. Cheng, M.-D, E. Corporan, M. DeWitt, C. Klingshirn, S.L. Allman, R. Striebich (2010) Use of Integrated Dilution Chamber and Membrane Thermodenuder for Measurement of Aircraft Engine VPM, The Annual SERDP Symposium, Washington, DC, November.
3. Cheng, M.-D. (2010) Measurement of Volatile Particles, the International Aerosol Congress, Helsinki, Finland, August.
4. Cheng, M.-D., E. Corporan, M. J. DeWitt, C. Klingshirn, S. Allman, and R. C. Striebich (2009) Use Integrated Dilution Chamber and Membrane Thermodenuder for Measurement of Aircraft Engine VPM, the Annual Symposium of SERDP/ESTCP, Washington, DC, November.
5. Cheng, Meng-Dawn, Edwin Corporan, and Matthew J. DeWitt (2009) Characteristics of Particles Emitted by Turbine Engine and In-Plume Conversion, Presented at the 2009 European Aerosol Conference in Karlsruhe, Germany, September.
6. Briones, A., J. Ervin, M. J. De Witt, S. Stouffer, C. Klingshirn, M.-D. Cheng, and E. Corporan (2008) A Numerical Investigation on the Performance of a Low-Flow Thermodenuder, the 4th Annual Dayton Engineering Science Symposium, ASME, Dayton, OH, October 27.